*toxins*

MDPI

*Article*

# *Pseudanabaena galeata* CCNP1313—Biological Activity and Peptides Production

**Marta Cegłowska [1,*], Karolina Szubert [2], Beata Grygier [3], Marzena Lenart [3], Jacek Plewka [3], Aleksandra Milewska [3], Kinga Lis [3,4], Artur Szczepański [3], Yuliya Chykunova [3], Emilia Barreto-Duran [3], Krzysztof Pyrć [3], Alicja Kosakowska [1] and Hanna Mazur-Marzec [2,*]**

1 Institute of Oceanology, Polish Academy of Sciences, Powstańców Warszawy 55, PL-81712 Sopot, Poland; akosak@iopan.gda.pl
2 Division of Marine Biotechnology, Institute of Oceanography, University of Gdańsk, M. J. Piłsudskiego 46, PL-81378 Gdynia, Poland; karolina.szubert@phdstud.ug.edu.pl
3 Virogenetics Laboratory of Virology, Małopolska Centre of Biotechnology, Jagiellonian University, Gronostajowa 7A, PL-30387 Cracow, Poland; beata.grygier@uj.edu.pl (B.G.); m.lenart@uj.edu.pl (M.L.); jacek.plewka@uj.edu.pl (J.P.); aleksandra.milewska@uj.edu.pl (A.M.); kinga1.lis@uj.edu.pl (K.L.); artur.szczepanski@uj.edu.pl (A.S.); y.chykunova@doctoral.uj.edu.pl (Y.C.); emilia.duran@uj.edu.pl (E.B.-D.); k.a.pyrc@uj.edu.pl (K.P.)
4 Faculty of Chemical Engineering and Technology, Cracow University of Technology, Warszawska 24, PL-31155 Cracow, Poland
* Correspondence: mceglowska@iopan.pl (M.C.); hanna.mazur-marzec@ug.edu.pl (H.M.-M.)

**Abstract:** Even cyanobacteria from ecosystems of low biodiversity, such as the Baltic Sea, can constitute a rich source of bioactive metabolites. Potent toxins, enzyme inhibitors, and anticancer and antifungal agents were detected in both bloom-forming species and less commonly occurring cyanobacteria. In previous work on the Baltic *Pseudanabaena galeata* CCNP1313, the induction of apoptosis in the breast cancer cell line MCF-7 was documented. Here, the activity of the strain was further explored using human dermal fibroblasts, African green monkey kidney, cancer cell lines (T47D, HCT-8, and A549$^{ACE2/TMPRSS2}$) and viruses (SARS-CoV-2, HCoV-OC43, and WNV). In the tests, extracts, chromatographic fractions, and the main components of the *P. galeata* CCNP1313 fractions were used. The LC-MS/MS analyses of the tested samples led to the detection of forty-five peptides. For fourteen of the new peptides, putative structures were proposed based on MS/MS spectra. Although the complex samples (i.e., extracts and chromatographic fractions) showed potent cytotoxic and antiviral activities, the effects of the isolated compounds were minor. The study confirmed the significance of *P. galeata* CCNP1313 as a source of metabolites with potent activity. It also illustrated the difficulties in assigning the observed biological effects to specific metabolites, especially when they are produced in minute amounts.

**Keywords:** *Pseudanabaena galeata*; cytotoxicity; anticancer activity; antiviral activity; new peptides

**Key Contribution:** *Pseudanabaena galeata* CCNP1313 exhibits potent cytotoxic and antiviral activity. The strain is also a source of new metabolites, the majority of which are variants of two different classes of peptides.



**Citation:** Cegłowska, M.; Szubert, K.; Grygier, B.; Lenart, M.; Plewka, J.; Milewska, A.; Lis, K.; Szczepański, A.; Chykunova, Y.; Barreto-Duran, E.; et al. *Pseudanabaena galeata* CCNP1313—Biological Activity and Peptides Production. *Toxins* **2022**, *14*, 330. https://doi.org/10.3390/toxins14050330

Received: 19 April 2022
Accepted: 3 May 2022
Published: 6 May 2022



## 1. Introduction

Cyanobacteria of the genus *Pseudanabaena* are classified to the Synechococcales order [1] and comprise almost fifty different species [2]. They live in various ecosystems, from marine and freshwater bodies to hot springs, mangrove swamps, and dry steppes [3–10]. Most of the published works have focused on the taxonomy and the presence of *Pseudanabaena* in different environments. In some studies, the effects of this cyanobacterium on other aquatic organisms have also been documented [8,11,12]. *Pseudanabaena* extracts were

found to be toxic to crustaceans: *Artemia salina* [8,12], *Daphnia magna* [11], and *Ceriodaphnia dubia* [11]. They also inhibited the growth of the marine alga *Nannochloropsis* sp. LEGE Z-004 and cyanobacterium *Synechococcus nidulans* LEGE 07171 [12]. As cellular extracts were used in these studies, the active agents could not be identified. Some *Pseudanabaena* chemotypes produce known toxins, such as microcystins [13–18], anatoxin-a [18], and saxitoxin [18]; therefore, these compounds could be responsible for the observed effects. *Pseudanabaena* has also been explored as a source of metabolites with biotechnological and pharmaceutical potential [19–22]. Extracts from different strains of *Pseudanabaena* were found to be active against herpes simplex type 2 virus (HSV-2) [19], reduced oxidative stress and cellular damage in renal cells [20], and inhibited the activity of α-glucosidase [22]. Costa et al. [21] described the effects of extracts from three Portuguese *Pseudanabaena* strains on cancer cells. In another screening study, the Baltic strain, *P. galeata* CCNP1313, was cytotoxic to the breast (MCF-7) and cervical (HeLa) cancer cell lines but did not affect human dermal fibroblasts (HDF) [23].

Here, the biological activity of the Baltic *P. galeata* CCNP1313 was further explored. For this purpose, cell extracts, chromatographic fractions, and the main components of the fractions were analyzed. Cytotoxicity of the samples was tested using several cell lines, including HDF, human breast adenocarcinoma (T47D), African green monkey kidney (Vero E6), human large intestine adenocarcinoma (HCT-8), and human lung epithelial cell lines overexpressing ACE2 and TMPRSS2 ($A549^{ACE2/TMPRSS2}$). In antiviral assays, severe acute respiratory syndrome coronavirus 2 (SARS-CoV-2), human coronavirus OC43 (HCoV-OC43), and West Nile virus (WNV) were used. The main components of the tested samples were characterized by liquid chromatography–tandem mass spectrometry (LC-MS/MS).

## 2. Results

### 2.1. Flash Chromatography and Peptide Separation

*P. galeata* CCNP1313 extract was first separated into thirty-one fractions using flash chromatography (Table S1). The fractions are marked as Fx.y, where x stands for MeOH (methanol) concentration and y is the number of the subsequent fractions eluted at x% MeOH. Additionally, four isolated peptides and four samples containing a mixture of 2–3 peptides were obtained (Table 1).

**Table 1.** The list of tested samples containing either isolated peptides or a mixture of 2–3 peptides obtained by preparative chromatography (runs P1–P3, fractions F20–80).

| Sample Number | *m*/*z* and Relative Amounts * (%) of the Peptides | Preparative (P) Chromatography Fractions | Weight (mg) |
|---|---|---|---|
| $A_1$ | 639 (75%), 862 (25%) | P1 F41 | 1.10 |
| $A_2$ | 656 (25%), 819 (60%), 854 (15%) | P1 F44–45 | 1.16 |
| $A_3$ | 730 (100%) | P1 F53–54 | 1.30 |
| $A_4$ | 726 (100%) | P1 F38 and P2 F19 | 1.10 |
| $A_5$ | 891 (100%) | P1 F87–90 | 1.21 |
| $A_6$ | 599 (32%), 716 (68%) | P2 F20–23 | 1.34 |
| $A_7$ | 677 (23%), 999 (77%) | P3 F39–40 | 0.70 |
| $A_8$ | 1167 (100%) | P3 F43–45 | 1.70 |

* The content of the compounds was assessed on the basis of the chromatographic peak area.

### 2.2. Bioactivity Screening

First, the activity of the cell extract from *P. galeata* CCNP1313 (200 μg $mL^{-1}$) was screened using a human breast adenocarcinoma cell line T47D and human dermal fibroblast HDF. The sample reduced the relative viability of T47D cells by 82% (SD = 1), but did not affect the primary HDF (toxicity below 1%). In the second step, the thirty-one flash chromatography fractions (200 μg $mL^{-1}$) obtained from the extract were tested against T47D cells. Twelve of the following fractions reduced the viability of T47D by more than 90%: F40.6–F40.7, F60.6–80.2, and F80.5–80.10 (Figure 1A). The same thirty-one fractions

were tested against HDF. Eleven of the fractions reduced the cell viability by more than 60%; these were fractions F60.2–F60.5, F60.7–F80.1, and F80.6–F80.10 (Figure 1B).

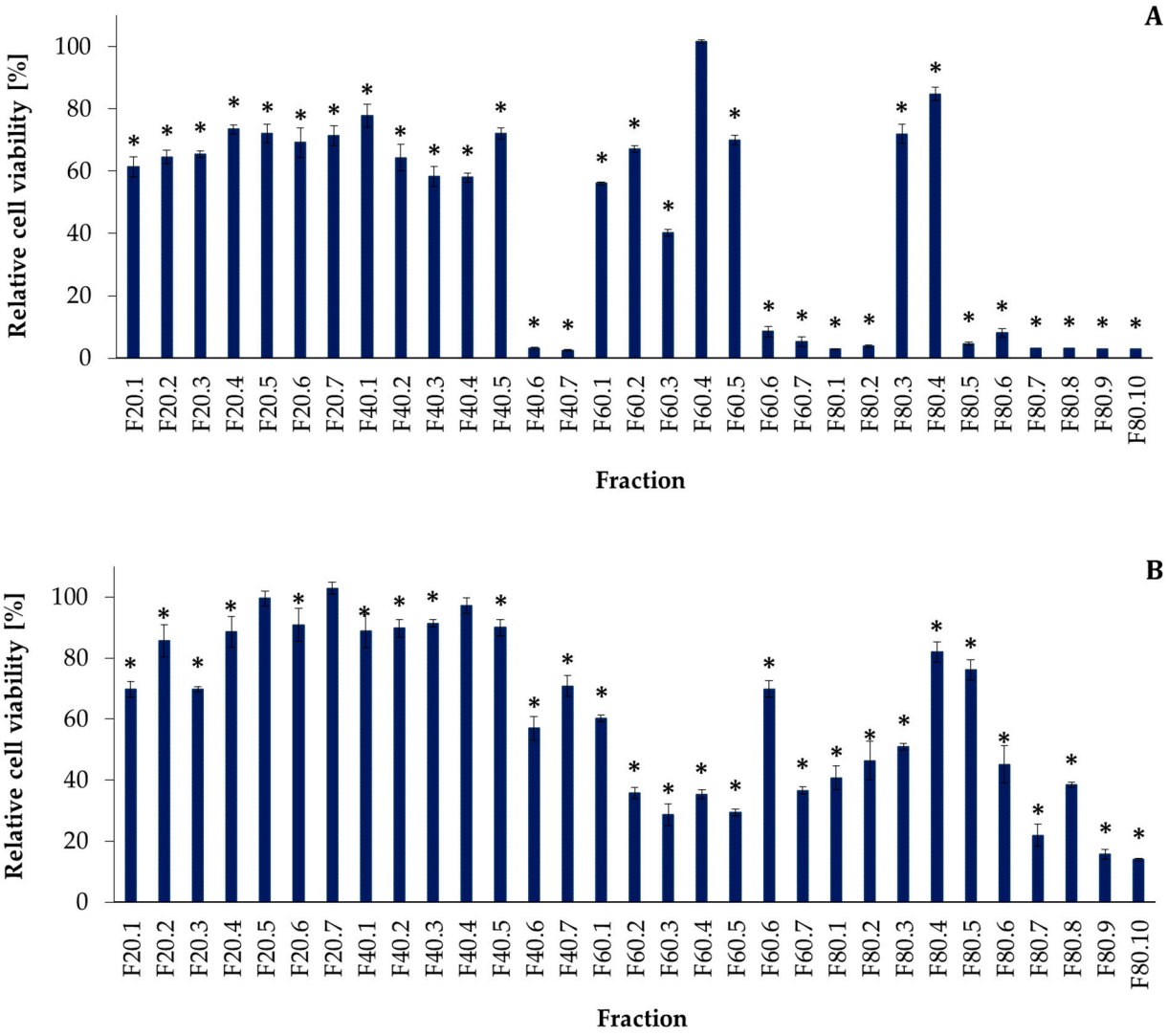


**Figure 1.** Effects of the *Pseudanabaena galeata* CCNP1313 flash chromatography fractions (200 µg mL$^{-1}$) on the relative viability of (**A**) human breast adenocarcinoma cells (T47D) and (**B**) human dermal fibroblasts (HDF). The statistical analyses were performed with the Student *t*-test. The significance is marked with * for $p < 0.05$. The fractions are marked as Fx.y, where x stands for MeOH concentration and y is the number of the subsequent fractions eluted at x% MeOH. Data are presented as mean values with standard deviation.

Then, the most active fractions were further separated and the samples with dominant components of the fractions were collected (Table 1) and tested against T47D and HDF. Neither of the samples affected the viability of T47D cells, but samples $A_2$, $A_4$, and $A_5$ were highly cytotoxic to the HDF (Figure 2). At the lowest concentration (25 µg mL$^{-1}$) the compounds reduced the HDF viability in a range from 56% (SD = 0; $CC_{50}$ lower than 25 µg mL$^{-1}$, $A_2$) to 73% (SD = 1; $CC_{50}$ lower than 25 µg mL$^{-1}$, $A_5$) (Figure 2). Sample $A_1$ was less active; however, the observed effects were dose-dependent. At the highest concentration (200 µg mL$^{-1}$), it reduced the cell viability by 60% (SD = 1). Samples $A_3$, $A_6$, and $A_8$ did not affect the viability of HDF (toxicity below 15% at 200 µg mL$^{-1}$) (Figure 2).

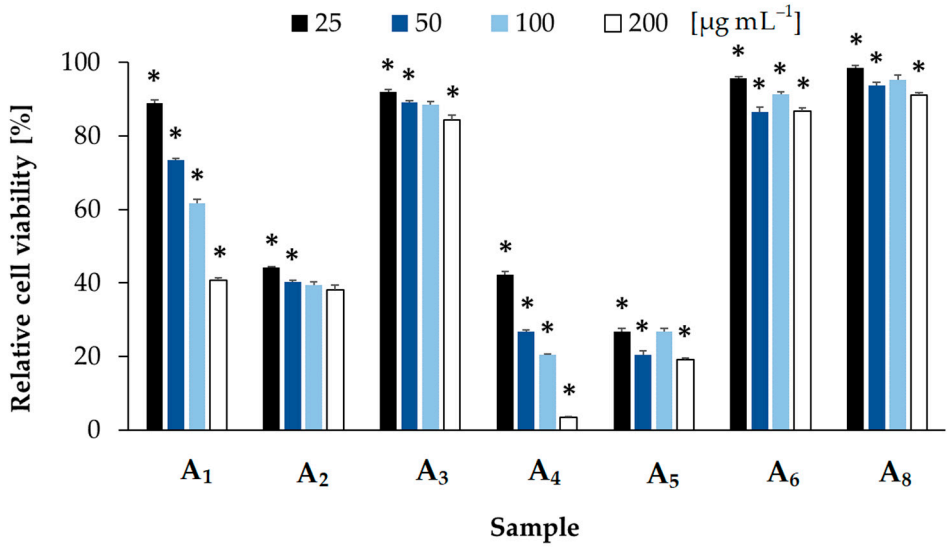


**Figure 2.** Effects of the isolated peptides ($A_3$–$A_5$ and $A_8$) and samples containing a mixture of 2–3 peptides ($A_1$, $A_2$ and $A_6$) from *Pseudanabaena galeata* CCNP1313 on the relative viability of the human dermal fibroblasts (HDF). The statistical analyses were performed using one-way ANOVA test. The significance is marked with * for $p < 0.05$; data are presented as mean values with standard deviation.

The antiviral activity of the *P. galeata* CCNP1313 cell extract was tested with the application of WNV, SARS-CoV-2, and HCoV-OC43. No cytopathic effects (CPE) were observed for HCT-8 cells infected with HCoV-OC43 and for Vero E6 cells infected with WNV. However, the extract was highly cytotoxic against Vero E6 cells infected with SARS-CoV-2. When the test was repeated with the extract roughly separated into four fractions (SPE F20–F80), the samples were not cytotoxic against Vero E6. Subsequently, reverse transcription (RT) and quantitative real-time PCR (RT-qPCR) were performed to assess the effect of the extract and SPE fractions on the viral RNA replication. The reduction in virus replication was expressed as a logarithmic reduction value (LRV) in the number of RNA copies in the infected cultures when compared to the untreated sample. The LRV for the tested viruses was equal to –1.7 (SD = 0.9) for WNV, –2.7 (SD = 0.7) for HCoV-OC43 (Figure S1), and from –0.3 (SD = 0.1) to –1.8 (SD = 0.3) for SARS-CoV-2 (Figure S2).

Next, the potential antiviral activity of the thirty-one flash chromatography fractions obtained from the *P. galeata* CCNP1313 cell extract was tested using SARS-CoV-2 and $A549^{ACE2/TMPRSS2}$ cells. First, the CPE reduction by the fractions was assessed in a range of concentrations (1, 10, and 50 μg $mL^{-1}$) (Table S2). Four fractions (F40.4, F40.5, F60.3, and F60.6), applied at the highest concentration, were toxic to $A549^{ACE2/TMPRSS2}$ cells. No virus-associated CPE were observed for fractions F20.7, F80.1, and F80.3–80.5 at 50 μg $mL^{-1}$. Additionally, fractions F20.6–F40.2, F40.6–F60.2, F80.1–F.80.3, and F80.5–F80.6 showed weak or no CPE at 10 and 50 μg $mL^{-1}$. For these samples, the effects on SARS-CoV-2 replication were examined by RT-qPCR. Three fractions F80.4–F80.6 decreased the LRV in a dose-dependent manner, and, when applied at 100 μg $mL^{-1}$, they reduced LRV by 3–4 $LOG_{10}$ (Figure 3). Antiviral effects were also observed for fractions F40.2 (LRV = −2.4, SD = 0.6), F40.6 (LRV = −2.2, SD = 1.4), F40.7 (LRV = −1.7, SD = 1.5), F60.1 (LRV = −2.2, SD = 1.4), F60.2 (LRV = −2.1, SD = 0.8), F80.2 (LRV = −1.6, SD = 0.7), and F80.3 (LRV = −2.4, SD = 1.0) (Figure 3).

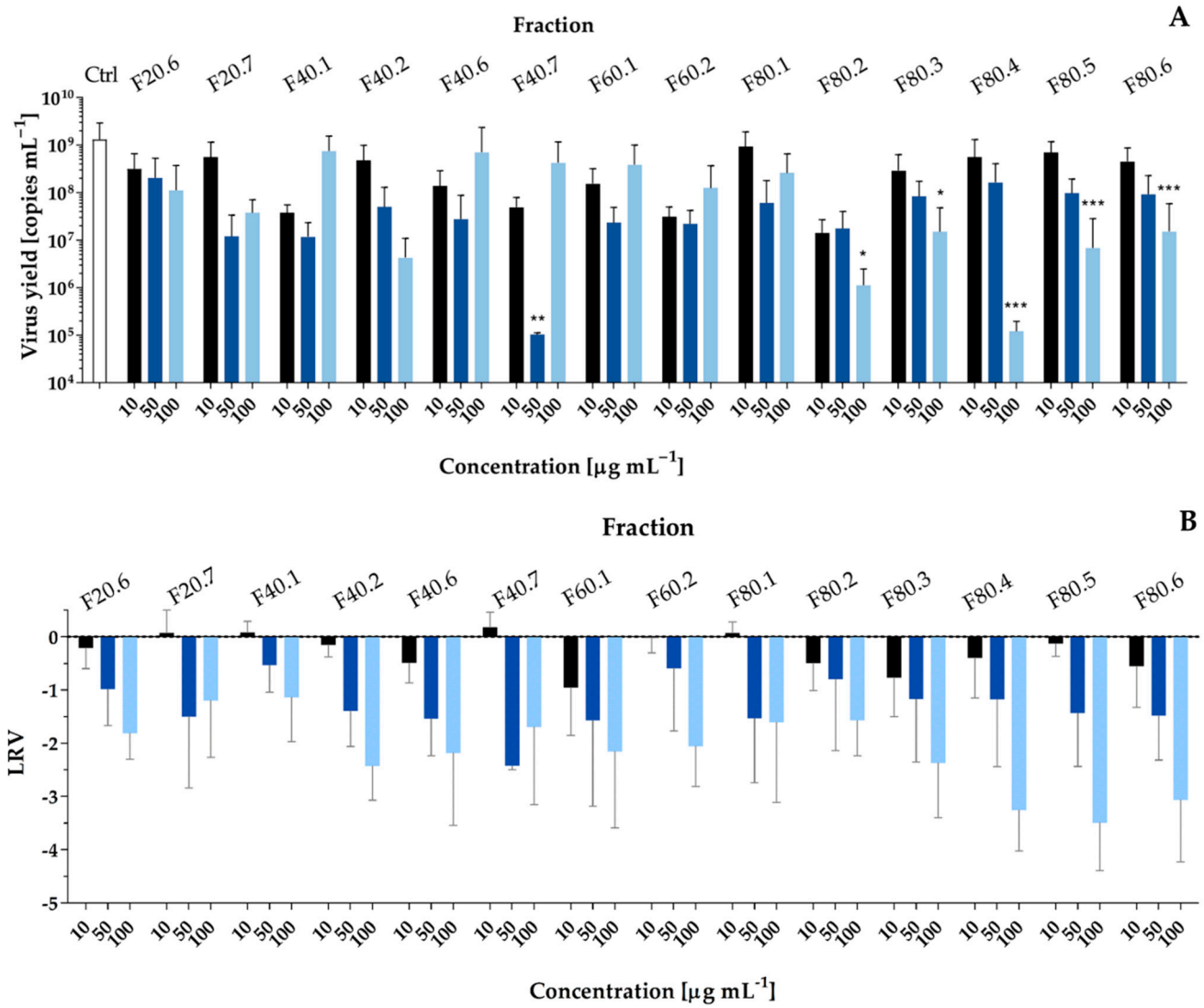


**Figure 3.** Antiviral activities of *Pseudanabaena galeata* CCNP1313 flash chromatography fractions against SARS-CoV-2 in A549$^{ACE2/TMPRSS2}$ cells (1600 TCID50 mL$^{-1}$; 96-h). The figure shows (**A**) the virus yield, analyzed by RT-qPCR, of the culture supernatants and (**B**) the logarithmic removal value (LRV) showing the relative decrease in the amount of the virus in the cell culture media compared to the untreated sample. Data are presented as mean values with standard deviation. The statistical analyses were performed with the Kruskal–Wallis test. The significance is marked with *** for $p < 0.001$, ** for $p < 0.01$ and * for $p < 0.05$. The fractions are marked as Fx.y, where x stands for MeOH concentration and y is the number of the subsequent fractions eluted at x% MeOH. Ctrl stands for viral control—untreated samples infected with the virus.

In the case of isolated peptides (sample $A_3$–$A_5$ and $A_8$) or samples containing a mixture of 2–3 petides ($A_1$–$A_2$, $A_6$, and $A_7$), a CPE reduction was recorded only for samples $A_2$, $A_3$, and $A_8$ at 100 µg mL$^{-1}$ (Table S3). These samples also had mild, but most significant effects on the SARS-CoV-2 replication (Sample $A_2$ LRV = −0.7, SD = 0.3; Sample $A_3$ LRV = −0.6, SD = 0.4; Sample $A_8$ LRV = −0.6, SD = 0.3) (Figure 4).

Next, selected samples (at 62.5 µg mL$^{-1}$ in the case of fractions and at 50 µg mL$^{-1}$ in the case of isolated peptides and samples containing 2–3 peptides) were screened for potential activities against the two main proteases of SARS-CoV-2, PL$^{pro}$ and M$^{pro}$, which are the viral proteins often targeted by antivirals (Tables S4–S6, Figures S3–S5). Fractions eluted with 80% MeOH (F80.2–F80.6) inhibited PL$^{pro}$ by more than 30%, with the most pronounced effects recorded for F80.5 (59%, SD = 7) (Table S4, Figure S3). The effects on

$M^{pro}$ were milder, and only for F40.7, F80.1, F80.4, and F80.5 was the inhibition slightly greater than 20% (Table S5, Figure S4). In the case of peptides or samples containing a mixture of 2–3 peptides, the strongest inhibition of $PL^{pro}$ was observed for samples $A_3$ (43%, SD = 34) and $A_4$ (40%, SD = 21) (Table S6, Figure S5).

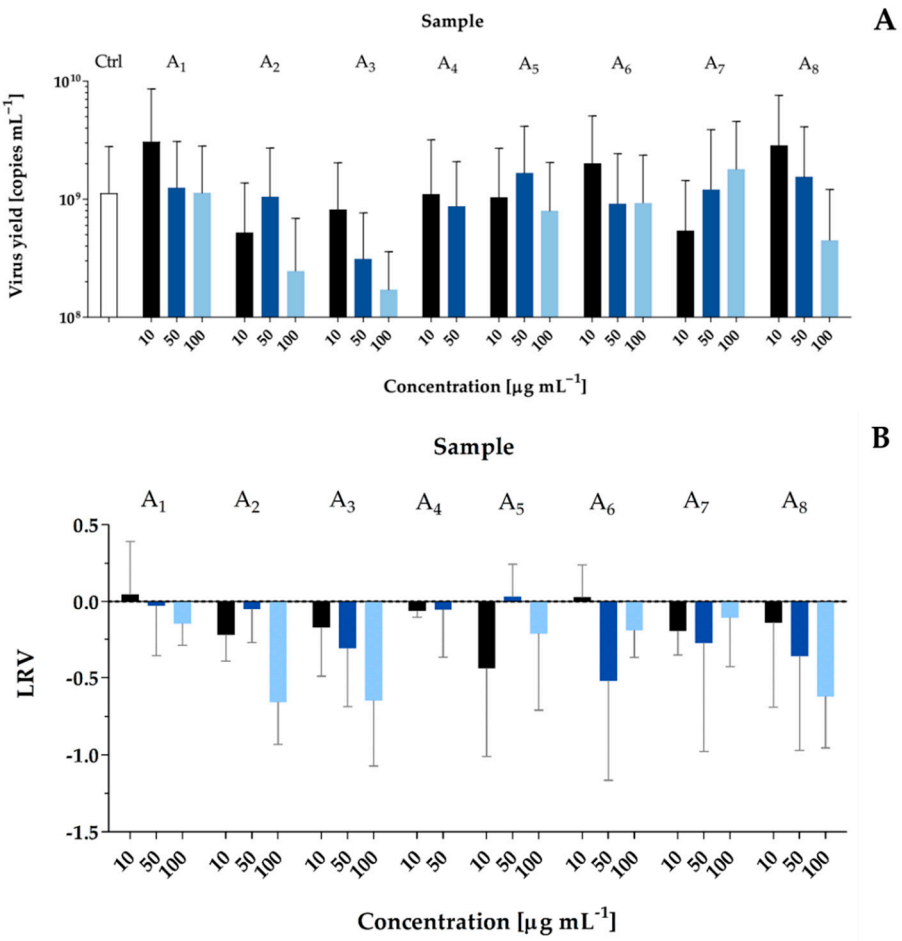


**Figure 4.** Antiviral activities of isolated peptides ($A_3$–$A_5$ and $A_8$) and samples containing a mixture of 2–3 peptides ($A_1$, $A_2$ and $A_6$) from *Pseudanabaena galeata* CCNP1313 against SARS-CoV-2 in $A549^{ACE2/TPMPRSS2}$ cells (1600 TCID50 $mL^{-1}$; 96-h). The figure shows (**A**) the virus yield, analyzed by RT-qPCR, of the cell culture supernatants and (**B**) the logarithmic removal value (LRV) showing the relative decrease in the amount of the virus in the cell culture media compared to the untreated sample. Data are presented as mean values with standard deviation. (The statistical analyses were performed with the Kruskal–Wallis test. No statistically significant differences were found). Ctrl stands for viral control—untreated samples infected with the virus.

### *2.3. Structure Characterization of Compounds Present in the Active Fractions*

In order to obtain sufficient amounts of material for bioassays, only the compounds present at the highest concentrations in the active fractions were isolated. Nontargeted LC-MS/MS analyses of the fractions revealed the presence of new peptides (Tables 2 and S1). For fourteen of the compounds, a tentative structure was suggested. De novo structure elucidation was performed manually based on collision-induced dissociation (CID) mass spectra of the precursor peptides. The spectra were reproducible and contained a high number of ion peaks. The presence of specific amino acid residues was deduced based on the immonium ion peaks and the mass differences between the subsequent high-intensity *b* ions, usually accompanied by the *a* ions. The *m*/*z* values of the pseudomolecular ions of the detected peptides ranged from 500 to 1183. The peptides contained proteinogenic residues, mainly with nonpolar side chains: Ile/Leu, Ala, Val, Phe, Pro, and Gly. The

presence of Arg, Ser, Met(O) (methionine sulfoxide), Met, Thr, or Tyr was rare. In the spectra of the Met(O)-containing peptides, a characteristic loss of 64 Da units was observed (Figures 5 and S7). It corresponds to methanesulfenic acid ($CH_3SOH$) present in a side chain of Met(O). The structure elucidation process is demonstrated in Figures 5–7, on the example of three peptides. Fragmentation spectra of the remaining peptides identified in *P. galeata* CCNP1313 are presented in the Supplementary Materials (Figures S6–S16). Because the applied method did not allow for discrimination between the isobaric ions of Leu and Ile, Leu * is used as a symbol of these residues. The structures of five of the compounds from samples $A_1$, $A_2$, $A_5$, $A_7$, and $A_8$ were not elucidated. However, the presence of characteristic immonium ions and differences between ion peaks allowed us to classify them as peptides. For the dereplication of tentatively identified structures, the CyanoMetDB database [24] was searched, but no matches were found. The detected peptides with at least two Ala residues, usually at the *N*- and *C*-termini, were marked as galeapeptins (GP), while Arg and Met-containing peptides were marked as PG (*Pseudanabaena galeata* peptides). The peptides with $m/z$ values 677, 854, 862 and 890, for which we were not able to suggest structures are marked as UP (unknown peptide).

**Table 2.** Suggested structures and activities of peptides detected in *Pseudanabaena galeata* CCNP1313 samples ((NT) indicates not tested; (–) indicates no activity; (+) indicates weak activity; (++) indicates mild activity; (+++) indicates strong activity).

| ***Pseudanabaena galeata* Peptides** | ***m/z*** | **Suggested Chemical Structure** | **Sample** | **Cytotoxic Activity** | | **Antiviral Activity** |
|---|---|---|---|---|---|---|
| | | | | **T47D** | **HDF** | |
| GP598 | 599 | Ala-Leu *-Val-Leu *-Leu *-Ala | $A_6$ | – | – | – |
| PG638 | 639 | Arg-MetO-Gly-Phe-Leu * | $A_1$ | – | + | – |
| GP655 | 656 | Ala-Leu *-Val-Leu *-Leu *-Ala-Gly | $A_2$ | – | ++ | + |
| UP676 | 677 | - | $A_7$ | NT | NT | – |
| PG709 | 710 | Arg-Met-Gly-Phe-Leu *-Ser | - | NT | NT | NT |
| GP715 | 716 | Ala-Val-Val-Phe-Leu *-Pro-Ala | $A_6$ | – | – | – |
| PG725 | 726 | Arg-MetO-Gly-Phe-Leu *-Ser | $A_4$ | – | +++ | – |
| GP729 | 730 | Ala-Pro-Val-Leu *-Phe-Leu *-Ala | $A_3$ | – | – | – |
| GP767 | 768 | Tyr-Ala-Ala-Phe-Leu *-Leu *-Ala | - | NT | NT | NT |
| GP794 | 795 | Ala-Val-Val-Leu *-Leu *-Pro-Leu *-Ala | - | NT | NT | NT |
| GP818 | 819 | Ala-Thr-Leu *-Val-Phe-Val-Val-Ala | $A_2$ | – | ++ | + |
| GP825 | 826 | Ala-Pro-Val-Leu *-?-Val-Leu *-Ala | - | NT | NT | NT |
| GP828 | 829 | Ala-Leu *-Val-Val-Leu *-Phe-Pro-Ala | - | NT | NT | NT |
| UP853 | 854 | - | $A_2$ | – | ++ | + |
| UP861 | 862 | - | $A_1$ | – | + | – |
| GP879 | 880 | Ala-Pro-Val-?-Pro-Ala-Val-Leu *-Ala | - | NT | NT | NT |
| UP890 | 891 | - | $A_5$ | – | +++ | – |
| GP998 | 999 | Ala-Pro-Val-Leu *-Ala-Phe-Val-Val-Leu *-Ala | $A_7$ | NT | NT | NT |
| GP1166 | 1167 | - | $A_8$ | – | – | + |

* Because the applied method did not allow for discrimination between the isobaric ions of Leu and Ile, Leu * is used as a symbol of these residues.

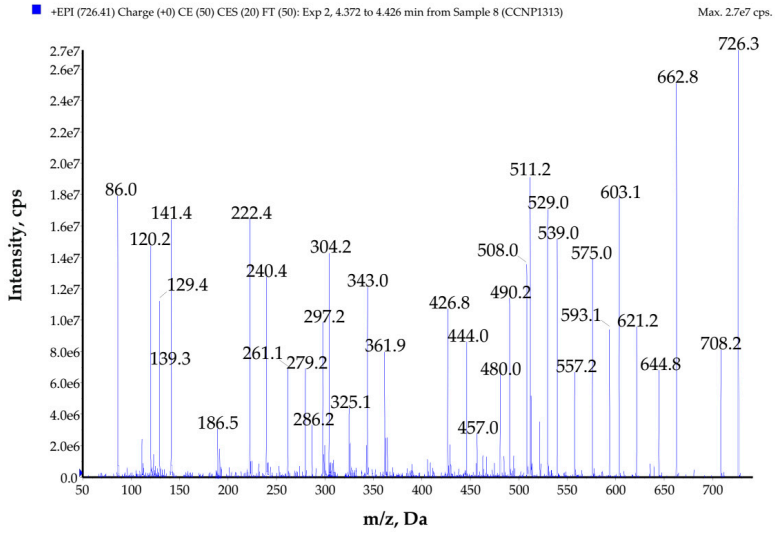


**Figure 5.** Enhanced product ion mass spectrum of the peptide named PG725 with the proposed structure Arg-MetO-Gly-Phe-Leu *-Ser, characterized based on the following ion peaks at $m/z$ **726** $[M + H]^+$, 708 $[M + H - H_2O]^+$, 662 $[M + H - CH_3SOH]^+$, 621 $[M + H - Ser]^+$, 603 $[M + H - Ser - H_2O]^+$, 593 $[M + H - Ser - CO]^+$, 575 $[M + H - Ser - CO - H_2O]^+$, 539 $[M + H - Ser - CH_3SOH - H_2O]^+$, 529 $[M + H - Ser - CH_3SOH - CO]^+$, 511 $[M + H - Ser - CH_3SOH - CO - H_2O]^+$, 508 $[M + H - (Leu * + Ser)]^+$, 490 $[M + H - (Leu * + Ser) - H_2O]^+$, 480 $[M + H - (Leu * + Ser) - CO]^+$, 444 $[M + H - (Leu * + Ser) - CH_3SOH]^+$, 361 $[M + H - (Phe + Leu * + Ser)]^+$, 343 $[M + H - (Phe + Leu * + Ser) - H_2O]^+$, 304 $[Arg + Met(O) + H]^+$, 297 $[M + H - (Phe + Leu * + Ser) - CH_3SOH]^+$, 286 $[Arg + Met(O) + H - H_2O]^+$, 279 $[M + H - (Phe + Leu * + Ser) - CH_3SOH - H_2O]^+$, 261 $[Phe + Leu * + H]^+$, 240 $[Arg + Met(O) + H - CH_3SOH]^+$, 222 $[Arg + Met(O) - CH_3SOH + H - H_2O]^+$, 141 $[Met(O) + Gly + H - CH_3SOH]^+$, 129 Arg immonium ion, 120 Phe immonium ion, 86 Leu * immonium ion.

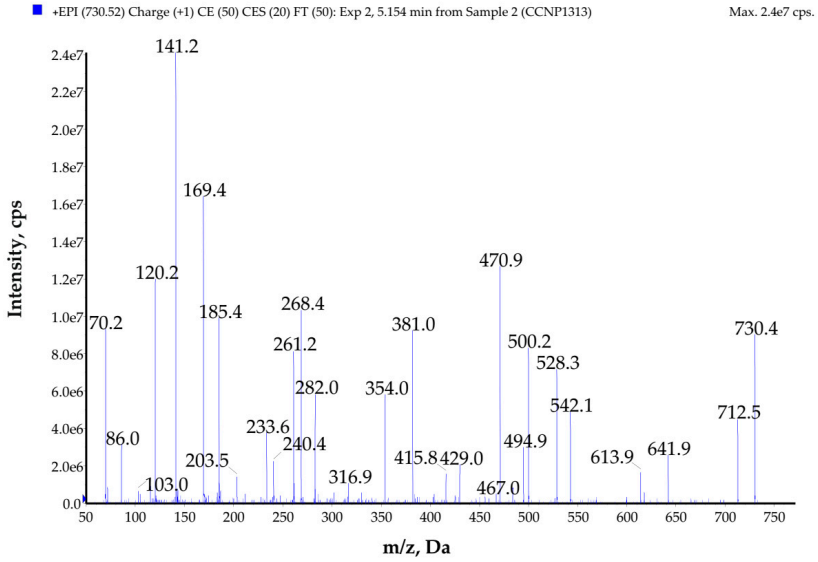


**Figure 6.** Enhanced product ion mass spectrum of galeapeptin GP729 with the proposed structure Ala-Pro-Val-Leu *-Phe-Leu *-Ala, characterized based on the following ion peaks at $m/z$ **730** $[M + H]^+$, 712 $[M + H - H_2O]^+$, 641 $[M + H - Ala]^+$, 613 $[M + H - Ala - CO]^+$, 542 $[Pro + Val + Leu * + Phe + Leu * - CO + H]^+$, 528 $[M + H - (Leu * + Ala)]^+$, 500 $[M + H - (Leu * + Ala) - CO]^+$, 429 $[Pro + Val + Leu * + Phe + H - CO]^+$, 381 $[M + H - (Phe + Leu * + Ala)]^+$, 353 $[M + H - (Phe + Leu * + Ala) - CO]^+$, 282 $[Pro + Val + Leu * + H - CO]^+$, 268 $[M + H - (Leu * + Phe + Leu * + Ala)]^+$, 261 $[Phe + Leu * + H]^+$, 240 $[M + H - (Leu * + Phe + Leu * + Ala) - CO]^+$, 233 $[Phe + Leu * + H - CO]^+$, 185 $[Val + Leu * + H - CO]^+$, 169 $[Ala + Pro + H]^+$, 141 $[Ala + Pro + H - CO]^+$, 120 Phe immonium ion, 86 Leu * immonium ion, 70 Pro immonium ion.

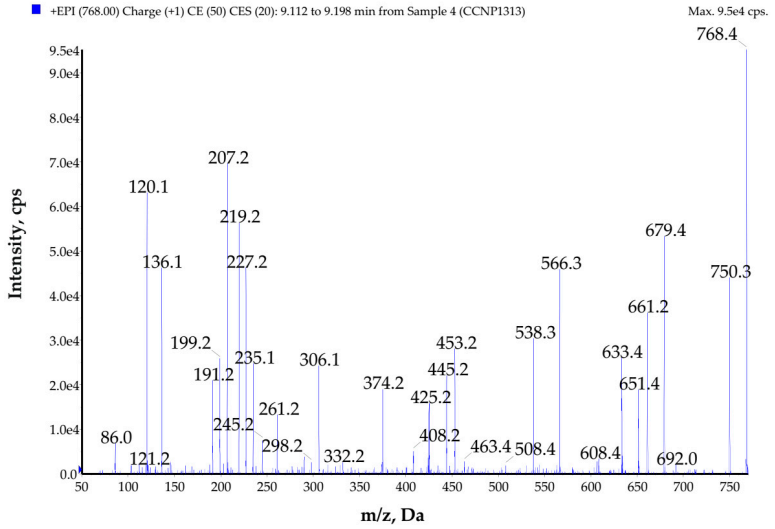


**Figure 7.** Enhanced product ion mass spectrum of galeapeptin GP767 with the proposed structure Tyr-Ala-Ala-Phe-Leu *-Leu *-Ala, characterized based on the following ion peaks at *m*/*z* **768** $[M + H]^+$, 750 $[M + H - H_2O]^+$, 679 $[M + H - Ala]^+$, 661 $[M + H - Ala - H_2O]^+$, 651 $[M + H - Ala - CO]^+$, 633 $[M + H - Ala - CO - H_2O]^+$, 566 $[M + H - (Leu * + Ala)]^+$, 538 $[M + H - (Leu * + Ala) - CO]^+$, 453 $[M + H - (Leu * + Leu * + Ala)]^+$, 445 $[Ala + Phe + Leu * + H]^+$, 425 $[M + H - (Leu * + Leu * + Ala) - CO]^+$, 374 $[Phe + Leu * + Leu * + H]^+$, 306 $[Tyr + Ala + Ala + H]^+$, 261 $[Phe + Leu * + H]^+$, 235 $[Tyr + Ala + H]^+$, 227 $[Leu * + Leu * + H]^+$, 219 $[Ala + Phe + H]^+$, 207 $[Tyr + Ala + H - CO]^+$, 199 $[Leu * + Leu * + H - CO]^+$, 191 $[Ala + Phe + H - CO]^+$, 136 Tyr immonium ion, 120 Phe immonium ion, 86 Leu * immonium ion.

## 3. Discussion

Among the various bioactive cyanobacterial products, compounds cytotoxic to human cancer cells were reported most frequently [25,26]. These compounds can cause inhibition of tubulin polymerization, microfilament disruption, caspase-3 activation, serine proteases inhibition or mitochondrial dysfunction, and oxidative damage [27,28]. One of the most successful cyanobacterial metabolites, dolastatin-10, was used as a lead structure to develop anticancer antibody-drug conjugates. Some of the conjugates have already been approved for cancer treatment, while others are still in clinical trials [29,30]. The antiviral activities of cyanometabolites were reported less frequently. Studies focused mainly on lectins, including cyanovirin-N (CV-N) and microvirin (MVN). These proteins bind with high affinity to oligomannose glycans of viral envelope glycoproteins gp120 [31,32]. Other antiviral agents include polysaccharides [33], peptides [34], alkaloids [35], and sulfoglycolipids [36]. Analyses of cyanobacterial metabolites performed with computational tools led to the identification of new potential antiviral agents. Deoxycylindrospermopsin showed the in silico potential to inhibit SARS-CoV-2 $M^{pro}$ and $PL^{pro}$ [35], while phycocyanobilin, phycoerythrobilin, phycourocilin, and folic acid from *Arthrospira* were suggested to inhibit the virus replication by interaction with the spike protein (S-protein) [37].

In the case of cytotoxic and antiviral activities, a significantly higher number of studies documented the effects of cyanobacterial extracts or fractionated samples than isolated metabolites with characterized structures [7,21,23,37,38]. Felczykowska et al. [23] analyzed several strains of Baltic cyanobacteria. They found that the extract from *P. galeata* CCNP1313 induced the death of the MCF-7 breast cancer cells by apoptosis, without necrotic changes or any effects on human dermal fibroblasts. Here, we showed that both the *P. galeata* CCNP1313 extract and fractions separated by the flash chromatography were active against another breast cancer cell line (T47D). As the most active fractions were separated by fractions with mild or no effects on T47D, it can be concluded that *P. galeata* CCNP1313 produces more than one metabolite with cytotoxic activity against breast cancer cells. Some of the active fractions also decreased HDF viability, but the trend in activity changes

between the fractions was different to that in the case of T47D. This suggests that different agents are responsible for the activities against the two cell lines. Unfortunately, neither of the isolated peptides was found to be active in the MTT assays with T47D cells. Meanwhile, samples $A_2$ (GP655, GP818, and UP853), $A_4$ (PG725) and $A_5$ (UP890) (Table 2) even at the lowest concentration (25 μg $mL^{-1}$), reduced HDF viability by almost 60% (Figure 2). All isolated compounds present in the three active samples were also detected in the fractions F40.6–F60.4 (Table S1) for which a significant decrease in HDF viability was observed (Figures 1B and 2). As the extract from *P. galeata* CCNP1313 was inactive against HDF, the positive results for some fractions and compounds isolated from the extract might be confusing. One of the possible reasons may be antagonistic interactions in complex samples that mask the activity of individual compounds.

Strong effects of *P. galeata* CCNP1313 metabolites on viral replication were recorded in the case of coronaviruses HCoV-OC43 and SARS-CoV-2, and flavivirus WNV. Due to the unpredictability of their prevalence, infectious properties, and lack of effective therapeutic and preventive medicines, the threat of global infections caused by both types of viruses is constantly increasing [39,40]. Since the emergence of coronavirus disease in 2019 (COVID-19) caused by SARS-CoV-2 [41], the research on this family of pathogens has intensified. This is also the reason why, in the current work, further studies were focused on the activity of *P. galeata* CCNP1313 metabolites against SARS-CoV-2. For this purpose, the human lung epithelial cell line $A549^{ACE2/TMPRSS2}$ overexpressing the angiotensin-converting enzyme 2 (ACE2), and the transmembrane serine proteases TMPRSS2, crucial for the SARS-CoV-2 spike protein priming was used [42,43]. $A549^{ACE2/TMPRSS2}$ cells recapitulate the natural route of entry for the coronavirus, which enters through fusion directly on the cell surface. As a result, this makes the virus independent of the endocytic machinery and cellular cathepsins [43]. Similarly to cytotoxic effects, the antiviral activity was recorded in fractions eluted with solvent of different MeOH content. They were separated by fractions that did not induce significant effects. This result, and the fact that only some of the fractions were active in both types of assays, indicate the production of several bioactive metabolites with selective activity against specific targets. $A549^{ACE2/TMPRSS2}$ cells infected with SARS-CoV-2 showed no or weak CPE when treated with fractions F40.2, F40.6–F60.2, and F80.3–F80.6 (Table S2). For the same fractions, the highest inhibition of viral replication was recorded. Furthermore, fractions F80.3–F80.6 showed the strongest inhibition of SARS-CoV-2 $PL^{pro}$ (Table S4, Figure S3). This papain-like protease encoded by the viral genome is one of the proteins that are essential for viral replication [44]. The protein also dysregulates the host immune sensing [45]. Small molecules, including FDA-approved drugs, have been extensively searched for their SARS $PL^{pro}$ inhibitory activity using high-throughput in vitro and in silico methods [44,46,47]. Although none of them has been approved yet, several $PL^{pro}$ inhibitors are currently in clinical trials, e.g., SPI-1005 (ClinicalTrials.gov Identifier: NCT04484025) and isotretinoin (ClinicalTrials.gov Identifier: NCT04361422).

Recognition of the biological activities of fractions containing a complex mixture of metabolites is just the first step, which should lead to the identification of the hits amongst *P. galeata* CCNP1313 metabolites. Therefore, in this study, the dominant components of the most active fractions were isolated and their activities were tested. The most profound CPE reduction and the concentration-dependent inhibition of viral replication were observed for sample $A_2$ containing GP655, GP818, and UP853; sample $A_3$ containing GP729 (136.9 μM); and sample $A_8$ containing GP1166 (85.7 μM) (Figure 4, Table S3). Based on the mass fragmentation spectra, four of the compounds (GP655, GP818, GP729, and GP1166) were classified to the same group of peptides. However, we were not able to elucidate the structure of GP1166. As this GP was also present in flash chromatography fractions showing some activity in antiviral assays (i.e., in F80.1–F80.3), this peptide may potentially be responsible for the observed effects.

Because no matches were found in the CyanoMetDB database [24] for the compounds detected in *P. galeata* CCNP1313 samples, they are considered new structures. None of them could also be classified as a new variant of the known peptides group commonly occurring

in cyanobacterial taxa. So far, the only peptides identified in *Pseudanabaena* species were microcystins [13–18]. Based on the analyses of MS/MS spectra it can be concluded that peptides detected in *P. galeata* CCNP1313 are composed of proteinogenic amino acids. In peptides with *m*/*z* 639 and 726 (named here PG638 and PG725), arginine and oxidized methionine were probably present. These two peptides have a similar structure and differ only in an additional Ser residue at the *C*-terminal part of PG725. The Met(O) present in the structure of these peptides can be an artefact formed in a nonenzymatic way during sample processing. It can also be a product of post-translational modifications generated by reactive oxygen species [48,49]. Here, the former option seems more probable as low amounts of the Met-containing variant of PG725, i.e., PG709, were also present in the extract and chromatographic fractions (Table 2, Table S1). In other compounds, mainly amino acids with hydrophobic side chains, such as those in Leu, Gly, Ala, Val, and Phe, were identified based on the immonium ions and mass differences in the MS/MS spectra.

Numerous peptides and peptide-like structures show a broad spectrum of biological activities. Generally, they are selective in their interactions with cellular targets, do not accumulate to toxic levels in organs, and can be easily synthesized or/and modified. Their therapeutic potential as anticancer peptides (ACPs) or antiviral peptides (AVPs) has been extensively explored, frequently with the application of computational screening techniques [46,50–53]. It was found that due to negatively charged components on the surface of the cancer cell, anticancer peptides should contain cationic amino acid residues (Lys or/and Arg) to facilitate the electrostatic interaction with the cell [54]. On the other hand, the hydrophobic parts of the peptides increase their membrane penetration capability. Therefore, in ACPs, Gly, Lys, and Leu were found to be the dominant components. The activity against cancer cells can also be enhanced by the presence of Pro, Phe, and Tyr [53,55]. Hydrophobic residues and their modifications belong to the main components of several known anticancer cyanobacterial peptide-like structures such as dolastatin-10 [56], apratoxins [57], cryptophycins [58], aurilides [59], and belamide A [60]. Ala, Gly, Leu *, Phe, Pro, and Val also dominate in the structure of the peptides detected in *P. galeata* CCNP1313 samples. Although the isolated peptides did not affect T47D, the results obtained for one cancer cell line cannot eliminate the compounds from the list of potential ACPs. Peptides can also target viral or host proteins. In the case of the SARS-CoV-2 spike protein, specific residues of the receptor-binding domain can interact with AVPs, mainly through hydrogen bonding and, to a lesser degree, through hydrophobic and electrostatic interactions [51]. For these interactions, the presence of Tyr, Phe, Pro, Gly, Leu, Ala, Asn, Gln, and Cys were found to be the most important [51,52]. Considering the above findings it can be speculated, that modification of *P. galeata* CCNP1313 peptide structures by the introduction of residues likely to form hydrogen bonds with the viral proteins could enhance the activity of the compounds. But even in their natural form, the isolated peptides possess some structural elements characteristic for both ACPs and AVPs, therefor the screening of their activity against a wider array of targets could shed more light on their pharmaceutical potential.

## 4. Conclusions

The studies conducted in this work and also the results previously published by Felczykowska et al. [23] proved the significance of *P. galeata* CCNP1313 as a source of potent cytotoxic and antiviral metabolites. Unfortunately, neither of the isolated peptides was found to be responsible for the cytotoxic activity against T47D. Some antiviral effects of the peptides were observed, but they were also weaker than that recorded for chromatographic fractions. It can be speculated that the bioactive metabolites produced by *P. galeata* CCNP1313 occur in minute amounts and/or were not detected with the applied LC-MS/MS method. The other option is that the observed effects resulted from interactions of several cell components present in complex samples and could not be restored in the case of single compounds.

## 5. Materials and Methods

### *5.1. Culture Conditions*

*P. galeata* CCNP1313 (GenBank accession number MN273769) [7] was grown for biomass in BG11 medium, at room temperature (22 ± 1 °C), with constant illumination (20 µM photons $m^{-2}$ $s^{-1}$) and aeration [61]. The biomass from 5-L cultures was harvested in the exponential growth phase by centrifugation (4000× *g*; 15 min; 4 °C) and lyophilized (Martin Christ Gefriertrocknungsanlagen, Osterode am Harz, Germany).

### *5.2. Extraction and Isolation of Metabolites*

The freeze-dried cyanobacterial material (2 g portions) was extracted twice with 75% methanol in MilliQ water (25 mL × 2) by vortexing (15 min) followed by bath sonication (2 min) and centrifugation (10,000× *g*; 15 min; 4 °C). The obtained supernatants were combined and diluted in MilliQ water so that the final MeOH concentration was reduced to less than 10%. The diluted extract was applied to a preconditioned 1 g Sep-Pak Vacc $tC_{18}$ cartridge (Waters, Milford, MA, USA) and the adsorbed substances were either eluted with 20 mL of 100% MeOH (crude extract) or with 20 mL of solvents composed of 20, 40, 60, and 80% MeOH in MilliQ water (SPE fractions). The eluates were evaporated to dryness in a centrifugal vacuum concentrator (MiVac, SP Scientific, Ipswich, UK) and tested in cytotoxicity and antiviral assays as extracts or SPE fractions.

To assess the activity of chromatographically separated fractions, 20 g of freeze-dried *P. galeata* CCNP1313 biomass was extracted twice with 500 mL of 75% MeOH as described above. The diluted extract was loaded onto a preconditioned 120 g SNAP KP-$C_{18}$-HS flash chromatography column (Biotage, Uppsala, Sweden) using a Shimadzu HPLC system (Shimadzu Corporation, Kyoto, Japan) equipped with a photodiode array detector (PDA) and a fraction collector. A step gradient of aqueous MeOH (20–80%) was used to elute the sample components. For each of the steps of the chromatographic gradient, seven (20%–60% MeOH) or ten (80% MeOH) 40-mL fractions were collected (Table S1). Absorbance was measured at 210 and 280 nm and the flow rate was 20 mL $min^{-1}$. Portions (5-mL) of each fraction were taken and concentrated in a centrifugal vacuum concentrator for two hours and then lyophilized.

From selected fractions collected during flash chromatography (Table 3) the dominant components were isolated by further fractionation using the same HPLC system but different columns (Table 3). The mobile phase was composed of 5% acetonitrile in MilliQ water (A) and 100% acetonitrile (B) both with 0.1% formic acid. The conditions of three preparative chromatography runs (Prep1–Prep3) are shown in Table 3. The components of the samples containing isolated peptides or a mixture of 2–3 peptides were characterized based on their mass fragmentation spectra (Table 1). Before the assays, the samples were vacuum concentrator and lyophilized.

**Table 3.** Chromatographic conditions used for the separation of the main components of the flash chromatography fractions obtained from the *Pseudanabaena galeata* CCNP1313 extract.

| | **Prep1** | **Prep2** | **Prep3** |
|---|---|---|---|
| | **Flash Chromatography Fractions** | | |
| | **F40%.7–F60%.3** | **F40%.2 and F40%.6** | **F80%.1–F80%.3** |
| Precolumn | SecurityGuard Prep Cartridge $C_{12}$ (15 × 30 mm; 90 Å; 4 µm) (Phenomenex, Torrence, CA, USA) | ReproSil-Pur Basic $C_{18}$ (5 × 4.6 mm; 100 Å; 5 µm) (Dr. Maisch GmbH, Ammerbuch, Germany) | |
| Column | Jupiter Proteo $C_{12}$ (250 × 21.2 mm; 90 Å; 4 µm) (Phenomenex, Torrence, CA, USA) Flow rate: 15 mL $min^{-1}$ | ReproSil-Pur Basic $C_{18}$ (250 × 4.6 mm; 100 Å; 5 µm) (Dr. Maisch GmbH, Ammerbuch, Germany) Flow rate: 1.5 mL $min^{-1}$ | |

**Table 3.** *Cont.*

| | Prep1 | Prep2 | Prep3 |
|---|---|---|---|
| | **Flash Chromatography Fractions** | | |
| | **F40%.7–F60%.3** | **F40%.2 and F40%.6** | **F80%.1–F80%.3** |
| Gradient | From 10% B to 100% B in 35 min | From 20% B to 100% B in 35 min | From 15% B to 100% B in 70 min |
| Fraction volume | 3 mL per vial | 1.5 mL per vial | 1.5 mL per vial |

### *5.3. LC-MS/MS Analyses*

At each step of extraction and fractionation, the contents of the samples were analyzed using a hybrid triple quadrupole/linear ion trap mass spectrometer (QTRAP5500, Applied Biosystems, Sciex, Concord, ON, Canada) coupled with an Agilent 1200 (Agilent Technologies, Waldboronn, Germany) HPLC system. The analyses were performed in a positive ion electrospray scanning mode, using a Zorbax Eclipse XDB-$C_{18}$ column (4.6 × 150 mm; 5 µm) (Agilent Technologies, Santa Clara, CA, USA) and the same mobile phase as in preparative chromatography [61]. Spectra within the range of $m/z$ of 500–1000 Da, and with signal intensity greater than 500,000 cps, were collected at a collision energy of 50 V. The results were processed using Analyst QS (Version 1.7.1, Applied Biosystems/MDS Analytical Technologies, Concord, ON, Canada, 2019).

### *5.4. Cytotoxicity Assays*

The evaluation of the cytotoxicity of *P. galeata* CCNP1313 was carried out in three steps. In the first step, the activity of the extract (200 µg $mL^{-1}$) against T47D and HDF was analyzed. In the second step, the activities of thirty-one flash chromatography fractions (200 µg $mL^{-1}$), were tested against T47D and HDF (both cell lines from the European Collection of Authenticated Cell Cultures (ECACC); Merck KGaA, Darmstadt, Germany). In the final step, the activities of samples $A_1$–$A_6$ and $A_8$ (25–200 µg $mL^{-1}$) against both cell lines were tested. MTT assays were performed according to Felczykowska et al. [23]. In summary, T47D cells were seeded in RPMI1640 medium (Carl Roth GmbH, Karlsruhe, Germany). HDF cells were seeded in Dulbecco's Modified Eagle Medium (DMEM) (Gibco, Thermo Fisher Scientific Inc., Waltham, MA, USA). Both media were supplemented with fetal bovine serum (10% $v/v$; Merck KGaA, Darmstadt, Germany) and penicillin–streptomycin solution (50 U and 50 µg $mL^{-1}$; Merck KGaA, Darmstadt, Germany). In the tests, the cells were seeded at 1 × $10^4$ cells per well and at each step of the test incubated at 37 °C, 5% $CO_2$. The cytotoxicity of fractions dissolved in 1% DMSO was measured after incubation (24 h) with the application of a microplate reader (Spectramax i3, Molecular Devices, LLC., San Jose, CA, USA). Cell viability was calculated as the ratio of the mean absorbance value for the three replicates containing the samples to the mean absorbance of the three replicates of the corresponding solvent control and expressed as a percentage with standard deviation. Data were analyzed using the Student *t*-test or one-way ANOVA test when applicable.

### *5.5. Antiviral Activity*

As in the case of cytotoxicity assays, the activities of extract, flash chromatography fractions and samples $A_1$–$A_8$ were analyzed.

Cell Culture. Vero E6 (ATCC: CRL-1586), HCT-8 (ATCC: CCL-244), primary human dermal fibroblasts, A549 (ATCC: CCL-185; ATCC, Manassas, VA, USA) overexpressing ACE2 and TMPRSS2 ($A549^{ACE2/TMPRSS2}$ in-house generated [43]) were maintained in DMEM medium (Gibco, Thermo Fisher Scientific Inc., Waltham, MA, USA) supplemented with 5% v/v heat-inactivated fetal bovine serum (FBS; Gibco, Thermo Fisher Scientific Inc., Waltham, MA, USA) and penicillin-streptomycin solution (100 U $mL^{-1}$ and 100 µg $mL^{-1}$, respectively) (PAN Biotech GmbH, Aidenbach, Bayern, Germany). Medium

for A549$^{ACE2/TMPRSS2}$ cells was additionally supplemented with blasticidin S (10 µg mL$^{-1}$; Sigma-Aldrich, Merck, Warsaw, Poland) and puromycin (0.5 µg mL$^{-1}$; Sigma-Aldrich, Merck, Warsaw, Poland).

Cytotoxicity Assays. The XTT Cell Viability Assay Kit (Biological Industries, Cromwell, CT, USA) was used according to the manufacturer's instructions. Briefly, cells were incubated with samples at different concentrations (10–250 µg mL$^{-1}$) for 48–120 h at 37 °C, 5% $CO_2$ (Table 4). After incubation, the medium was discarded and fresh medium was overlaid on the cells, along with the activated 2,3-bis-(2-methoxy-4-nitro-5-sulfophenyl)-(2H)-tetrazolium-5-carboxanilide (XTT) solution and the cells were incubated for 2 h (37 °C, 5% $CO_2$). The absorbance was measured using a microplate reader (Tecan Infinite M200; Tecan Group Ltd., Männedorf, Switzerland). Only extracts exhibiting low cytotoxicity (the viability of the treated >80% compared to the untreated samples) were further analyzed.

**Table 4.** Infection models and tested *Pseudanabaena galeata* CCNP1313 samples.

| Virus | Cells | Infection Culture Condition | Samples |
|---|---|---|---|
| **WNV** strain Hungary 578/10 $TCID_{50}$ = 400 mL$^{-1}$ | Vero E6 | 37 °C, 5% $CO_2$, 48 h | Extract; 250 µg mL$^{-1}$ |
| **HCoV-OC43** ATCC: VR-1558 $TCID_{50}$ = 400 mL$^{-1}$ | HCT-8 | 32 °C, 5% $CO_2$, 96–120 h | Extract; 250 µg mL$^{-1}$ |
| **SARS-CoV-2** $TCID_{50}$ = 400 mL$^{-1}$ PL_P18 [GISAID Clade G, Pangolin lineage B.1] (accession numbers for the GISAID database: EPI_ISL_451979) | Vero E6 | 37 °C, 5% $CO_2$, 72 h | F20, F40, F60, F80; 50 µg mL$^{-1}$ |
| **SARS-CoV-2** $TCID_{50}$ = 1600 mL$^{-1}$ PL_P18 [GISAID Clade G, Pangolin lineage B.1] (accession numbers for the GISAID database: EPI_ISL_451979) | A549$^{ACE2/TMPRSS2}$ | 37 °C, 5% $CO_2$, 96 h | Flash chromatography fractions; samples $A_1$–$A_8$; 10, 50, 100 µg mL$^{-1}$ |

Cytopathic Effects Assessment. The cytopathic effects were assessed with the application of a light microscope (Evos Fluorescent Microscope, Thermo Fisher Scientific Inc., Waltham, MA, USA) 96-h post-infection (p.i.).

Virus Replication Inhibition Assays. Cells were preincubated with different concentrations of the samples (2 h, 37 °C, 5% $CO_2$; Table 4). The virus infection was then performed in the presence of the samples (Table 4). After 2 h, cells were rinsed twice with PBS and a fresh medium with another portion of the tested samples was added. After 48–120 h infection (Table 4) the CPE caused by the virus in the cell monolayer was evaluated, and the culture supernatants were collected for RT-qPCR analyses of viral replication.

RNA Isolation and RT-qPCR. The isolation of viral RNA was carried out using a commercially available RNA isolation kit (Viral DNA/RNA Isolation Kit; A&A Biotechnology, Gdańsk, Poland), according to the protocol provided by the manufacturer. The isolated RNA was subjected to RT-qPCR using the GoTaq® Probe 1-Step RT-qPCR System Protocol kit (Promega, Madison, WI, USA) according to the manufacturer's instructions with the use of primers and probes (Genomed, Warsaw, Poland) listed in Table 5. Appropriate standards were prepared to evaluate the number of viral RNA molecules in the samples. The reaction was carried out in a thermal cycler (CFX96 Touch Real-197 Time PCR Detection System; Bio-Rad, Hercules, CA, USA). The obtained data are presented as LRV, showing the relative decrease in the amount of virus in the cell culture media compared to the untreated

sample. Data were analyzed using the nonparametric Mann–Whitney or Kruskal–Wallis tests when applicable.

**Table 5.** Oligonucleotides used in RT-qPCR.

| Virus | Oligonucleotides | Sequence (5′ -> 3′) |
|---|---|---|
| **ZIKV** | Primer 5′ (Forward) | TTGGTCATGATACTGCTGATTGC |
| | Primer 3′ (Reverse) | CCTTCCACAAAGTCCCTATTGC |
| | Probe | 6-FAM-CGGCATACAGCATCAGGTGCATAGGAG-TAMRA |
| **WNV** | Primer 5′ (Forward) | CGGAAGTyGrGTAkACGGTGCTG |
| | Primer 3′ (Reverse) | CGGTwyTGAGGGCTTACrTGG |
| | Probe | 6-FAM-wCCCCAGGwGGACTG-BHQ1 |
| **HCoV-OC43** | Primer 5′ (Forward) | AGCAACCAGGCTGATGTCAATACC |
| | Primer 3′ (Reverse) | AGCAGACCTTCCTGAGCCTTCAAT |
| | Probe | 6-FAM-TGACATTGTCGATCGGGACCCAAGTA-TAMRA |
| **SARS-CoV-2** | Primer 5′ (Forward) | CACATTGGCACCCGCAATC |
| | Primer 3′ (Reverse) | GAGGAACGAGAAGAGGCTTG |
| | Probe | 6-ACTTCCTCAAGGAACAACATTGCCA-BHQ-1 |

Inhibition of SARS-CoV-2 proteases. In the assays, the following reagents were used: $M^{pro}$ and $PL^{pro}$ from in-house production [62,63], TRIS (Bioshop, Burlington, Ontario, Canada), NaCl (Bioshop), BSA (Bioshop), DTT (Bioshop), DMSO (Sigma-Aldrich, Merck, Warsaw, Poland), synthetic peptidic $M^{pro}$ substrate Ac-VKLQ-(AMC), synthetic peptidic $Pl^{pro}$ substrate Ac-RLRGG-(AMC) (Enzo, New York, NY, USA). The enzymatic activities of the SARS-CoV-2 proteases $M^{pro}$ and $PL^{pro}$ were tested for protein at the final concentration of 160 nM in 50 mM Tris pH 8, 150 mM NaCl, 0.01% BSA, 5 mM DTT buffer, and 120 nM in 50 mM Tris pH 8, 150 mM NaCl, 0.01% BSA, 10 mM DTT buffer, respectively.

For the assay, the protein solution (10 µL) was first loaded onto a low-volume white 96-well plate and incubated for 1 h at room temperature with 0.2 µL of inhibitors solution. The experiment was carried out in duplicate. The enzymatic reaction was started by adding 10 µL of substrate equipped with 7-amino-4-methylcoumarin (AMC) fluorophore at a final concentration of 50 µM and 2 µM, respectively. Enzymatic activity was assessed determining the changes in the fluorescence, using Tecan M200 Pro (Tecan Group Ltd., Männedorf, Switzerland). The signal was measured at 360/460 nm excitation/emission wavelengths for 90 min with 60 s intervals and with 2 s orbital shaking after each measurement. Data analyses were performed using Mathematica 12 (Wolfram, Oxfordshire, UK).

The percentage of inhibition was calculated as a fraction of the initial velocity of the $M/PL^{pro}$ control according to the formula:

$$100\% - \frac{\text{initial velocity with inhibitor}}{\text{initial velocity M/PLpro control}}$$

The initial velocities were calculated by fitting a straight line into datapoints from 20 to 30 using a script in Mathematica12 software. Enzymatic assays were validated using well-known $PL^{pro}$ (GRL0617 ($IC_{50}$: 2.1 µM) [64]) and $M^{pro}$ inhibitors (PF-07321332, commercial name—nirmatrelvir ($IC_{50}$: 19.2 nM), ClinicalTrials.gov Identifier: NCT05263908) (Figure S17).

**Supplementary Materials:** The following supporting information can be downloaded at: https://www.mdpi.com/article/10.3390/toxins14050330/s1. Table S1: The content of the *Pseudanabaena galeata* CCNP1313 flash chromatography fractions. Figure S1: Antiviral activities of the *Pseudanabaena galeata* CCNP1313 crude extract against human coronavirus OC43 (HCoV-OC43) in HCT-8 cells and

West Nile Virus (WNV) in Vero E6 cells. The figure shows (A) virus yield, analyzed by RT-qPCR, of cell culture supernatants and (B) logarithmic removal value (LRV) showing the relative decrease in the amount of the virus in the cell culture media compared to the untreated samples. Ctrl stands for viral control—untreated samples infected with the virus. Data are presented as mean values with standard deviation; the statistical analyses were performed with the Mann—Whitney test. The significance is marked with * for $p < 0.05$. Figure S2: Antiviral activities of the *Pseudanabaena galeata* CCNP1313 solid-phase extraction (SPE) fractions against severe acute respiratory syndrome coronavirus 2 (SARS-CoV-2) in Vero E6 cells. The figure shows (A) virus yield, analyzed by RT-qPCR, of cell culture supernatants and (B) the logarithmic removal value (LRV) showing the relative decrease in the amount of the virus in the cell culture media compared to the untreated sample. Ctrl stands for viral control—untreated samples infected with the virus. Data are presented as mean values with standard deviation; the statistical analyses were performed with the Kruskal–Wallis test. The significance is marked with * for $p < 0.05$. Table S2: The cytopathic effects (CPE) of the *Pseudanabaena galeata* CCNP1313 flash chromatography fractions after SARS-CoV-2 infection of the $A549^{ACE2/TMPRSS2}$ cell line. The CPE was assessed microscopically after 96-h from the infection ($TCID_{50}$ = 1600 $mL^{-1}$ based on the following scale: (+++) indicates no reduction of infection-induced CPE, comparable to the positive control; (++) indicates 20–40% reduction of infection-induced CPE; (+) indicates 50–70% reduction of infection-induced CPE; (−) indicates maximal infection reduction, comparable to the mock-infected samples (+/−) indicates an uncertain CPE; (tox) indicates toxicity). Table S3: The cytopathic effects (CPE) of isolated peptides ($A_3$–$A_5$ and $A_8$) and samples containing a mixture of 2–3 peptides ($A_1$, $A_2$ and $A_6$) from *Pseudanabaena galeata* CCNP1313 after SARS-CoV-2 infection of the $A549^{ACE2/TMPRSS2}$ cell line. The CPE was assessed microscopically after 96-h from the infection ($TCID_{50}$ = 1600 $mL^{-1}$ based on the following scale: (+++) indicates no reduction of infection-induced CPE, comparable to the positive control; (++) indicates 20–40% reduction of infection-induced CPE; (+) indicates 50–70% reduction of infection-induced CPE; (−) indicates maximal infection reduction, comparable to the mock-infected samples. (NT) indicates not tested). Table S4: The effects of selected *Pseudanabaena galeata* CCNP1313 flash chromatography fractions on the activity of SARS-CoV-2 $PL^{Pro}$ protease. Data are presented as mean values with standard deviation. Figure S3: The effects of selected *Pseudanabaena galeata* CCNP1313 flash chromatography fractions on the activity of SARS-CoV-2 $PL^{Pro}$ protease. The fractions are marked as Fx.y, where x stands for MeOH concentration and y is the number of the subsequent fractions eluted at x% MeOH. Data are presented as mean values. Table S5: The effects of selected *Pseudanabaena galeata* CCNP1313 flash chromatography fractions on the activity of SARS-CoV-2 $M^{Pro}$ protease. inhibition fractions. Data are presented as mean values with standard deviation. Figure S4: The effects of selected *Pseudanabaena galeata* CCNP1313 flash chromatography fractions on the activity of SARS-CoV-2 $M^{Pro}$ protease. The fractions are marked as Fx.y, where x stands for MeOH concentration and y is the number of the subsequent fractions eluted at x% MeOH. Data are presented as mean values. Table S6: The effects of isolated peptides and samples containing a mixture of 2–3 peptides from *Pseudanabaena galeata* CCNP1313 on the activity of SARS-CoV-2 $PL^{Pro}$ protease. Data are presented as mean values with standard deviation. Figure S5: The effects of isolated peptides and samples containing a mixture of 2–3 peptides from *Pseudanabaena galeata* CCNP1313 on the activity of SARS-CoV-2 $PL^{Pro}$ protease. Figure S6: Enhanced product ion mass spectrum of galeapeptin GP598 with the proposed structure Ala-Leu *-Val-Leu *-Leu *-Ala, characterized based on the following ion peaks at $m/z$ 599 $[M + H]^+$, 581 $[M + H - H_2O]^+$, 510 $[M + H -$ Ala $*]^+$, 483 $[M + H -$ Ala $- CO]^+$, 397 $[M + H -$ (Leu * + Ala$]^+$/[Ala + Leu * + Val + Leu * + $H]^+$, 369 [Ala + Leu * + Val + Leu * + $H - CO]^+$, 284 [Ala + Leu * + Val + $H]^+$, 266 [Ala + Leu * + Val $- H_2O + H]^+$, 256 [Ala + Leu * + Val $-$ CO + $H]^+$, 213 [Leu * + Val + $H]^+$, 185 [Ala + Leu * + $H]^+$/[Leu * + Val $-$ CO + $H]^+$, 157 [Leu * + Ala $-$ CO + $H]^+$, 86 Leu * immonium ion, 72 Val immonium ion. Figure S7: Enhanced product ion mass spectrum of a peptide named PG638 with the proposed structure Arg-MetO-Gly-Phe-Leu *, characterized based on the following ion peaks at $m/z$ 639 $[M + H]^+$, 621 $[M + H - H_2O]^+$, 575 $[M + H - CH_3SOH]^+$, 508 $[M + H -$ Leu $*]^+$, 490 $[M + H -$ Leu * $- H_2O]^+$, 480 $[M + H -$ Leu * $- H_2O]^+$, 444 $[M + H -$ Leu * $- CH_3SOH]^+$, 426 $[M + H -$ Leu * $- CH_3SOH - H_2O]^+$, 416 $[M + H -$ Leu * $- CH_3SOH - CO]^+$, 398 $[M + H -$ Leu * $- CH_3SOH - H_2O - CO]^+$, 361 $[M + H -$ (Phe + Leu *)$]^+$, 343 $[M + H -$ (Phe + Leu *) $- H_2O]^+$, 304 [Arg + Met(O) + $H]^+$, 297 $[M + H - CH_3SOH -$ (Phe + Leu *)$]^+$, 286 [Arg + Met(O) + $H - H_2O]^+$, 279 $[M + H - CH_3SOH -$ (Phe + Leu *) $- H_2O]^+$, 240 [Arg + Met(O) + $H - CH_3SOH]^+$, 222 [Arg + Met(O) + $H - CH_3SOH - H_2O]^+$, 141 [Met(O) + Gly + $H - CH_3SOH]^+$, 129 Arg immonium ion, 120 Phe immonium ion, 86 Leu * immonium ion. Figure S8: Enhanced product ion mass spectrum of

the galeapeptin GP655 with the proposed structure Ala- Leu *-Val-Leu *-Leu *-Ala-Gly, characterized based on the following ion peaks at $m/z$ 656 $[M + H]^+$, 638 $[M + H - H_2O]^+$, 581 $[M + H - Gly]^+$, 563 $[M + H - Gly - H_2O]^+$, 553 $[M + H - Gly - CO]^+$, 510 [Ala + Leu * + Val + Leu * + Leu * + H]$^+$, 492 [Ala + Leu * + Val + Leu * + Leu * + H $- H_2O]^+$, 482 [Ala + Leu * + Val + Leu * + Leu * + H $- CO]^+$, 397 $[M + H - (Leu * + Ala + Gly)]^+$/[Ala + Leu * + Val + Leu * + H]$^+$, 369 [Ala + Leu * + Val + Leu * + H $- CO]^+$, 284 [Ala + Leu * + Val + H]$^+$, 266 [Ala + Leu * + Val + H $- H_2O]^+$, 256 [Ala + Leu * + Val + H $- CO]^+$, 213 [Leu * + Val + H]$^+$, 195 [Leu * + Val + H $- H_2O]^+$, 185 [Ala + Leu * + H]$^+$/[Leu * + Val + H $- CO]^+$, 167 [Ala + Leu * + H $- H_2O]^+$, 157 [Leu * + Ala + H $- CO]^+$, 86 Leu * immonium ion, 72 Val immonium ion. Figure S9: Enhanced product ion mass spectrum of peptide a peptide named PG709 with the proposed structure Arg-Met-Gly-Phe-Leu *-Ser, characterized based on the following ion peaks at $m/z$ 710 $[M + H]^+$, 692 $[M + H - H_2O]^+$, 682 $[M + H - CO]^+$, 605 $[M + H -$ Ser$]^+$, 587 $[M + H -$ Ser $- H_2O]^+$, 577 $[M + H -$ Ser $- CO]^+$, 559 $[M + H -$ Ser $- CO - H_2O]^+$, 492 $[M + H - (Leu * +$ Ser$)]^+$, 474 $[M + H - (Leu * +$ Ser$) - H_2O]^+$, 464 $[M + H - (Leu * +$ Ser$) - CO]^+$, 446 $[M + H - (Leu * +$ Ser$) - H_2O - CO]^+$, 345 [Arg + Met + Gly + H]$^+$, 327 [Arg + Met + Gly + H $- H_2O]^+$, 270 [Arg + Met + H $- H_2O]^+$, 129 Arg immonium ion, 120 Phe immonium ion, 86 Leu * immonium ion. Figure S10: Enhanced product ion mass spectrum of galeapeptin GP715 with the proposed structure Ala-Val-Val-Phe-Leu *-Pro-Ala, characterized based on the following ion peaks at $m/z$ 716 $[M + H]^+$, 627 $[M + H -$ Ala$]^+$, 599 $[M + H -$ Ala $- CO]^+$, 530 $[M + H - (Pro +$ Ala$)]^+$, 502 $[M + H - (Pro +$ Ala$) - CO]^+$, 460 [Val + Val + Phe + Leu * + H]$^+$, 432 [Val + Val + Phe + Leu * + H $- CO]^+$, 417 $[M + H - (Leu * +$ Pro + Ala$)]^+$, 389 $[M + H - (Leu * +$ Pro + Ala$) - CO]^+$, 346 [Val + Val + Phe + H]$^+$, 318 [Val + Val + Phe + H $- CO]^+$, 270 [Ala + Val + Val + H]$^+$, 261 [Phe + Leu * + H]$^+$, 247 [Val + Phe + H]$^+$, 233 [Phe + Leu * + H $- CO]^+$, 219 [Val + Phe + H $- CO]^+$, 211 [Leu * + Pro + H]$^+$, 199 [Val + Val + H]$^+$, 171 [Ala + Val + H]$^+$, 143 [Ala + Val + H $- CO]^+$, 120 Phe immonium ion, 86 Leu * immonium ion, 72 Val immonium ion, 70 Pro immonium ion. Figure S11: Enhanced product ion mass spectrum of galeapeptin G794 with the proposed structure Ala-Val-Val- Leu *-Leu *-Pro-Leu *-Ala, characterized based on the following ion peaks at $m/z$ 795 $[M + H]^+$, 706 $[M + H -$ Ala$]^+$, 678 $[M + H -$ Ala $- CO]^+$, 593 $[M + H - (Leu * +$ Ala$)]^+$, 565 $[M + H - (Leu * +$ Ala$) - CO]^+$, 496 $[M + H - (Pro +$ Leu * + Ala$)]^+$, 468 $[M + H - (Pro +$ Leu * + Ala$) - CO]^+$, 383 [Ala + Val + Val + Leu * + H]$^+$, 355 [Ala + Val + Val + Leu * + H $- CO]^+$, 324 [Leu * + Leu * + Pro + H]$^+$, 270 [Ala + Val + Val + H]$^+$, 211 [Leu * + Pro + H]$^+$, 199 [Leu * + Leu * + H $- CO]^+$, 183 [Leu * + Pro + H $- CO]^+$, 171 [Ala + Val + H]$^+$, 143 [Ala + Val + H $- CO]^+$, 86 Leu * immonium ion, 72 Val immonium ion, 70 Pro immonium ion. Figure S12: Enhanced product ion mass spectrum of galeapeptin GP818 with the proposed structure Ala-Thr-Leu *-Val-Phe-Val-Val-Ala, characterized based on the following ion peaks at $m/z$ 819 $[M + H]^+$, 801 $[M + H - H_2O]^+$, 730 $[M + H -$ Ala$]^+$, 712 $[M + H -$ Ala $- H_2O]^+$, 702 $[M + H -$ Ala $- CO]^+$, 684 $[M + H -$ Ala $- H_2O - CO]^+$, 631 $[M + H - (Val +$ Ala$)]^+$, 613 $[M + H - (Val +$ Ala$) - H_2O]^+$, 603 $[M + H - (Val +$ Ala$) - CO]^+$, 532 $[M + H - (Val +$ Val + Ala$)]^+$, 514 $[M + H - (Val +$ Val + Ala$) - H_2O]^+$, 504 $[M + H - (Val +$ Ala$) - CO]^+$, 367 $[M + H - (Phe -$ Val + Val + Ala$) - H_2O]^+$, 213 [Leu * + Val + H]$^+$, 185 [Ala + Leu * + H]$^+$, 157 [Ala + Leu * + H $- CO]^+$, 171 [Val + Val + H $- CO]^+$, 120 Phe immonium ion, 86 Leu * immonium ion, 74 Thr immonium ion, 72 Val immonium ion. Figure S13: Enhanced product ion mass spectrum of galeapeptin GP825 with the proposed partially elucidated structure Ala-Pro-Val-Leu *-?-Val-Leu *-Ala, characterized based on the following ion peaks at $m/z$ 826 $[M + H]^+$, 808 $[M + H - H_2O]^+$, 737 $[M + H -$ Ala$]^+$, 624 $[M + H - (Leu * +$ Ala$)]^+$, 596 $[M + H - (Leu * +$ Ala$) - CO]^+$, 525 $[M + H - (Val +$ Leu * + Ala$)]^+$, 497 $[M + H - (Val +$ Leu * + Ala$) - CO]^+$, 381 [Ala + Pro + Val + Leu * + H]$^+$, 353 [Ala + Pro + Val + Leu * + H $- CO]^+$, 268 [Ala + Pro + Val + H]$^+$, 169 [Ala + Pro + H]$^+$, 141 [Ala + Pro + H $- CO]^+$, 120 Phe immonium ion, 86 Leu * immonium ion. Figure S14: Enhanced product ion mass spectrum of galeapeptin GP828 with the proposed structure Ala-Leu *-Val-Val-Leu *-Phe-Pro-Ala, characterized based on the following ion peaks at $m/z$ 829 $[M + H]^+$, 740 $[M + H -$ Ala$]^+$, 712 $[M + H -$ Ala $- CO]^+$, 643 $[M + H - (Pro +$ Ala$)]^+$, 625 $[M + H - (Pro +$ Ala$) - H_2O]^+$, 615 $[M + H - (Pro +$ Ala$) - CO]^+$, 572 $[M + H -$ Ala $- (Pro +$ Ala$)]^+$, 544 $[M + H -$ Ala $- (Pro +$ Ala$) - CO]^+$, 496 $[M + H - (Pro +$ Ala$)]^+$, 468 $[M + H - (Pro +$ Ala$) - CO]^+$, 383 [Ala + Leu * + Val + Val + H]$^+$, 355 [Ala + Leu * + Val + Val + H $- CO]^+$, 312 [Leu * + Val + Val + H]$^+$, 284 [Ala + Leu * + Val + H]$^+$, 213 [Leu * + Val + H]$^+$, 185 [Leu * + Val + H $- CO]^+$/ [Ala + Leu * + H]$^+$, 199 [Val + Val + H]$^+$, 157 [Ala + Leu * + H $- CO]^+$, 171 [Val + Val + H $- CO]^+$, 120 Phe immonium ion, 86 Leu * immonium ion, 72 Val immonium ion, 70 Pro immonium ion. Figure S15: Enhanced product ion mass spectrum of galeapeptin GP879 with the proposed partially elucidated structure Ala-Pro-Val-?-Pro-Ala-Val-Leu *-Ala, characterized based on the following ion peaks at $m/z$ 880 $[M + H]^+$, 862 $[M + H - H_2O]^+$, 791 $[M + H -$ Ala$]^+$, 773 [M +

H − Ala − $H_2O$]$^+$, 678 [M + H − (Leu * + Ala)]$^+$, 660 [M + H − (Leu * + Ala) − $H_2O$]$^+$, 650 [M + H − (Leu * + Ala) − CO]$^+$, 632 [M + H − (Leu * + Ala) − $H_2O$ − CO]$^+$, 579 [M + H − (Val + Leu * + Ala)]$^+$, 561 [M + H − (Val + Leu * + Ala) − $H_2O$]$^+$, 551[M + H − (Val + Leu * + Ala) − $H_2O$ − CO]$^+$, 508 [M + H − (Ala + Val + Leu * + Ala)]$^+$, 411 [M + H − (Pro + Ala + Val + Leu * + Ala)]$^+$, 393 [M + H − (Pro + Ala + Val + Leu * + Ala) − $H_2O$]$^+$, 383 [M + H − (Pro + Ala + Val + Leu * + Ala) − CO]$^+$, 381 [Ala + Pro + Val + Leu * + H]$^+$, 365 [M + H − (Pro + Ala + Val + Leu * + Ala) − $H_2O$ − CO]$^+$, 353 [Ala + Pro + Val + Leu * + H − CO]$^+$, 268 [Ala + Pro + Val + H]$^+$, 169 [Ala + Pro + H]$^+$, 141 [Ala + Pro + H − CO]$^+$, 120 Phe immonium ion, 86 Leu * immonium ion. Figure S16: Enhanced product ion mass spectrum of galeapeptin GP998 with the proposed structure Ala-Pro-Val-Leu *-Ala-Phe-Val-Val-Leu *-Ala, characterized based on the following ion peaks at *m*/*z* 999 [M + H]$^+$, 981 [M + H − $H_2O$]$^+$, 910 [M + H − Ala *]$^+$, 882 [M + H − Ala − CO]$^+$, 797 [M + H − (Leu * + Ala)]$^+$, 769 [M + H − (Leu * + Ala) − CO]$^+$, 698 [M + H − (Val + Leu * + Ala)]$^+$, 599 [M + H − (Val + Val + Leu * + Ala)]$^+$, 571 [M + H − (Val + Val + Leu * + Ala) − CO]$^+$, 530 [Val + Leu * + Ala + Phe + Val + H]$^+$, 452 [Ala + Pro + Val + Leu * + Ala + H]$^+$, 431 [Val + Leu * + Ala + Phe + H]$^+$, 417 [Ala + Phe + Val + Val +H]$^+$, 403 [Val + Leu * + Ala + Phe + H − CO]$^+$, 381 [Ala + Pro + Val + Leu * + H]$^+$, 353 [Ala + Pro + Val + Leu * + H - CO]$^+$, 332 [Leu * + Ala + Phe + H]$^+$, 268 [Ala + Pro + Val + H]$^+$, 219 [Ala + Phe + H]$^+$, 213 [Val + Leu * + H]$^+$, 199 [Val + Val + H]$^+$, 185 [Val + Leu * − CO + H]$^+$, 171 [Val + Val + H − CO]$^+$, 169 [Ala + Pro + H]$^+$, 141 [Ala + Pro + H − CO]$^+$, 120 Phe immonium ion, 86 Leu * immonium ion, 72 Val immonium ion. Figure S17: Positive controls and $IC_{50}$ values determination for enzymatic assays (A) $M^{pro}$ ($IC_{50}$ for PF-07321332 a well-known $M^{pro}$ inhibitor, commercial name nirmatrelvir with reported literature $IC_{50}$ value of 19.2 nM) and (B) $PL^{pro}$ ($IC_{50}$ determination for GRL-0617, a well-known $PL^{pro}$ inhibitor with reported literature $IC_{50}$ value of 2.1 μM).

**Author Contributions:** Conceptualization, M.C. and H.M.-M.; methodology, M.C., H.M.-M.; formal analysis, M.C., K.S., B.G., M.L., A.M., J.P. and A.S.; investigation, M.C., H.M.-M., K.S., B.G., M.L., J.P., A.S., K.L., Y.C. and E.B.-D.; resources, H.M.-M., M.C. and A.K.; writing—original draft preparation, M.C.; writing—review and editing, M.C., H.M.-M., B.G., M.L., J.P., K.S., A.K. and K.P.; visualization, M.C. and B.G.; supervision, H.M.-M.; project administration, H.M.-M.; funding acquisition, H.M.-M. and A.K. All authors have read and agreed to the published version of the manuscript.

**Funding:** This study was funded by the National Science Centre in Poland (project number NCN 2019/33/B/NZ9/02018 to HMM), and by the statutory program of the Institute of Oceanology, PAN (grant No. II.3).

**Institutional Review Board Statement:** Not applicable.

**Informed Consent Statement:** Not applicable.

**Data Availability Statement:** Not applicable.

**Conflicts of Interest:** The authors declare no conflict of interest.

## References

1. Komárek, J.; Kastovsksy, J.; Mares, J.; Johnsen, J. Taxonomic classification of Cyanoprokaryotes (cyanobacterial genera) 2014, using a polyphasic approach. *Preslia* **2014**, *86*, 295–335.
2. Guiry, M.D.; Guiry, M.D.; Guiry, G.M. (Eds.) *AlgaeBase*; World-Wide Electronic Publication; National University of Ireland: Galway, Ireland, 2022; Available online: http://www.algaebase.org (accessed on 18 April 2022).
3. Krienitz, L.; Ballot, A.; Casper, P.; Kotut, K.; Wiegand, C.; Pflugmacher, S. Cyanobacteria in hot springs of East Africa and their potential toxicity. *Algol. Stud.* **2005**, *117*, 297–306. [CrossRef]
4. Kirkwood, A.E.; Henley, E.J. Algal community dynamics and halotolerance in a terrestrial, hypersaline environment. *J. Phycol.* **2006**, *42*, 537–547. [CrossRef]
5. Matuła, J.; Pietryka, M.; Richter, D.; Wojtun, B. Cyanoprokaryota and algae of Arctic terrestrial ecosystems in the Hornsund area, Spitsbergen. *Pol. Polar Res.* **2007**, *28*, 283–315.
6. Molisani, M.M.; Barroso, H.D.; Becker, H.B.; Moreira, M.O.; Hijo, C.A.; Maia, T.D.; Harrison, G.R. Trophic state, phytoplankton assemblages and limnological diagnosis of the Castanhão reservoir, CE, Brazil. *Acta Limnol. Bras.* **2010**, *22*, 1–12. [CrossRef]
7. Mazur-Marzec, H.; Błaszczyk, A.; Felczykowsk, A.; Hohlfeld, N.; Kobos, J.; Toruńska-Sitarz, A.; Devi, P.; Montalvão, S.; D'souza, L.; Tammela, P.; et al. Baltic cyanobacteria—A source of biologically active compounds. *Eur. J. Phycol.* **2015**, *50*, 343–360. [CrossRef]
8. Mohamed, Z.A.; Al-Shehri, A.M. Biodiversity and toxin production of cyanobacteria in mangrove swamps in the Red Sea off the southern coast of Saudi Arabia. *Bot. Mar.* **2015**, *58*, 23–34. [CrossRef]

9. Yu, G.; Zhu, M.; Chen, Y.; Pan, W.; Chai, W.; Li, R. Polyphasic characterization of four species of Pseudanabaena (Oscillatoriales, cyanobacteria) from China and insights into polyphyletic divergence within the Pseudanabaena genus. *Phytotaxa* **2015**, *192*, 1–12. [CrossRef]
10. Temraleeva, A.D. Cyanobacterial diversity in the soil of Russian dry steppes and semideserts. *Microbiology* **2018**, *87*, 249–260. [CrossRef]
11. Olvera-Ramírez, R.; Centeno-Ramos, C.; Martínez-Jerónimo, F. Toxic effects of *Pseudanabaena tenuis* (Cyanobacteria) on the cladocerans *Daphnia magna* and *Ceriodaphnia dubia*. *Hidrobiologica* **2010**, *20*, 203–212.
12. Leão, P.N.; Ramos, V.; Gonçalves, P.B.; Viana, F.; Lage, O.M.; Gerwick, W.H.; Vasconcelos, V.M. Chemoecological screening reveals high bioactivity in diverse culturable Portuguese marine cyanobacteria. *Mar. Drugs* **2013**, *11*, 1316–1335. [CrossRef] [PubMed]
13. Oudra, B.; Loudiki, M.; Sbiyyaa, B.; Martins, R.; Vasconcelos, V.; Namikoshi, N. Isolation, characterization and quantification of microcystins (heptapeptides hepatotoxins) in *Microcystis aeruginosa* dominated bloom of Lalla Takerkoust lakereservoir (Morocco). *Toxicon* **2001**, *39*, 1375–1381. [CrossRef]
14. Oudra, B.; Loudiki, M.; Vasconcelos, V.; Sabour, B.; Sbiyyaa, B.; Oufdou, K.; Mezrioui, N. Detection and quantification of microcystins from cyanobacteria strains isolated from reservoirs and ponds in Morocco. *Environ. Toxicol.* **2002**, *17*, 32–39. [CrossRef] [PubMed]
15. Maršálek, B.; Bláha, L.; Babica, P. Analyses of microcystins in the biomass of *Pseudanabaena limnetica* collected in Znojmo reservoir. *Fottea* **2003**, *3*, 195–197.
16. Douma, M.; Loudiki, M.; Oudra, B.; Mouhri, K.; Ouahid, Y.; del Campo, F.F. Taxonomic diversity and toxicological assessment of cyanobacteria in Moroccan inland waters. *Rev. Des Sci. De L'eau/J. Water Sci.* **2009**, *22*, 435–449. [CrossRef]
17. Gantar, M.; Sekar, R.; Richardson, L.L. Cyanotoxins from black band disease of corals and from other coral reef environments. *Microb. Ecol.* **2009**, *58*, 856–864. [CrossRef] [PubMed]
18. Teneva, I.; Mladenov, R.; Dzhambazov, B. Toxic effects of extracts from *Pseudanabaena galeata* (Cyanoprokaryota) in mice and cell cultures in vitro. *Nat. Sci. Hum.* **2009**, *12*, 237–243.
19. Patterson, G.M.L.; Baker, K.K.; Baldwin, C.L.; Bolis, C.M.; Caplan, F.R.; Larsen, L.K.; Levine, I.A.; Moore, R.E.; Moore, E.; Nelson, C.S.; et al. Antiviral activity of cultured blue-green algae (Cyanophyta). *J. Phycol.* **1993**, *29*, 125–130. [CrossRef]
20. Cano-Europa, E.; Ortiz-Butrón, R.; Gallardo-Casas, C.A.; Blas-Valdivia, V.; Pineda-Reynoso, M.; Olvera-Ramírez, R.; Franco-Colin, M. Phycobiliproteins from *Pseudanabaena tenuis* rich in c-phycoerythrin protect against $HgCl_2$-caused oxidative stress and cellular damage in the kidney. *J. Appl. Phycol.* **2010**, *22*, 495–501. [CrossRef]
21. Costa, M.; Garcia, M.; Costa-Rodrigues, J.; Costa, M.S.; Ribeiro, M.J.; Fernandes, M.H.; Barros, P.; Barreiro, A.; Vasconcelos, V.; Martins, R. Exploring bioactive properties of marine cyanobacteria isolated from the Portuguese coast: High potential as a source of anticancer compounds. *Mar. Drugs* **2014**, *12*, 98–114. [CrossRef]
22. Priatni, S.; Budiwati, T.A.; Ratnaningrum, D.; Kosasih, W.; Andryani, R.; Susanti, H.; Susilaningsih, D. Antidiabetic screening of some Indonesian marine cyanobacteria collection. *Biodiversitas* **2016**, *17*, 642–646. [CrossRef]
23. Felczykowska, A.; Pawlik, A.; Mazur-Marzec, H.; Toruńska-Sitarz, A.; Narajczyk, M.; Richert, M.; Węgrzyn, G.; Herman-Antosiewicz, A. Selective inhibition of cancer cells' proliferation by compounds included in extracts from Baltic Sea cyanobacteria. *Toxicon* **2015**, *8*, 1–10. [CrossRef] [PubMed]
24. Jones, M.R.; Pinto, E.; Torres, M.A.; Dörr, F.; Mazur-Marzec, H.; Szubert, K.; Tartaglione, L.; Dell'Aversano, C.; Miles, C.O.; Beach, D.G.; et al. CyanoMetDB, a comprehensive public database of secondary metabolites from cyanobacteria. *Water Res.* **2021**, *196*, 117017. [CrossRef] [PubMed]
25. Dittmann, E.; Gugger, M.; Sivonen, K.; Fewer, D.P. Natural product biosynthetic diversity and comparative genomics of the cyanobacteria. *Trends Microbiol.* **2015**, *23*, 642–652. [CrossRef] [PubMed]
26. Demay, J.; Bernard, C.; Reinhardt, A.; Marie, B. Natural products from cyanobacteria: Focus on beneficial activities. *Mar. Drugs* **2019**, *17*, 320. [CrossRef] [PubMed]
27. Costa, M.; Costa-Rodrigues, J.; Fernandes, M.H.; Barros, P.; Vasconcelos, V.; Martins, R. Marine cyanobacteria compounds with anticancer properties: A review on the implication of apoptosis. *Mar. Drugs* **2012**, *10*, 2181–2207. [CrossRef]
28. Salvador-Reyes, L.A.; Luesch, H. Biological targets and mechanisms of action of natural products from marine cyanobacteria. *Nat. Prod. Rep.* **2015**, *32*, 478–503. [CrossRef]
29. Singh, S.B. Discovery and development of dolastatin 10-derived antibody drug conjugate anticancer drugs. *J. Nat. Prod.* **2022**, *85*, 666–687. [CrossRef]
30. Yang, K.; Chen, B.; Gianolio, D.D.; Stefano, J.E.; Busch, M.; Manning, C.; Alving, K.; Gregory, R.C.; Brondyk, W.H.; Miller, R.J.; et al. Convergent synthesis of hydrophilic monomethyl dolastatin 10 based drug linkers for antibody-drug conjugation. *Org. Biomol. Chem.* **2019**, *17*, 8115–8124. [CrossRef]
31. Helle, F.; Wychowski, C.; Vu-Dac, N.; Gustafson, K.R.; Voisset, C.; Dubuisson, J. Cyanovirin-N inhibits hepatitis C virus entry by binding to envelope protein glycans. *J. Biol. Chem.* **2006**, *281*, 25177–25183. [CrossRef]
32. Lotfi, H.; Sheervalilou, R.; Zarghami, N. An update of the recombinant protein expression systems of cyanovirin-N and challenges of preclinical development. *Bioimpacts* **2018**, *8*, 139–151. [CrossRef] [PubMed]
33. Mader, J.; Gallo, A.; Schommartz, T.; Handke, W.; Nagel, C.-H.; Günther, P.; Brune, W.; Reich, K. Calcium spirulan derived from *Spirulina platensis* inhibits herpes simplex virus 1 attachment to human keratinocytes and protects against herpes labialis. *J. Allergy Clin. Immunol.* **2016**, *137*, 197–203.e3. [CrossRef] [PubMed]

34. Zainuddin, E.N.; Mentel, R.; Wray, V.; Jansen, R.; Nimtz, M.; Lalk, M.; Mundt, S. Cyclic depsipeptides, ichthyopeptins A and B, from *Microcystis ichthyoblabe*. *J. Nat. Prod.* **2007**, *70*, 1084–1088. [CrossRef] [PubMed]
35. Naidoo, D.; Roy, A.; Kar, P.; Mutanda, T.; Anandraj, A. Cyanobacterial metabolites as promising drug leads against the $M^{pro}$ and $PL^{pro}$ of SARS-CoV-2: An in silico analysis. *J. Biomol. Struct. Dyn.* **2021**, *39*, 6218–6230. [CrossRef] [PubMed]
36. Loya, S.; Reshef, V.; Mizrachi, E.; Silberstein, C.; Rachamim, Y.; Carmeli, S.; Hizi, A. The inhibition of the reverse transcriptase of HIV-1 by the natural sulfoglycolipids from cyanobacteria: Contribution of different moieties to their high potency. *J. Nat. Prod.* **1998**, *61*, 891–895. [CrossRef] [PubMed]
37. Ferreira, L.; Morais, J.; Preto, M.; Silva, R.; Urbatzka, R.; Vasconcelos, V.; Reis, M. Uncovering the bioactive potential of a cyanobacterial natural products library aided by untargeted metabolomics. *Mar. Drugs* **2021**, *19*, 633. [CrossRef] [PubMed]
38. Petit, L.; Vernès, L.; Cadoret, J.-P. Docking and in silico toxicity assessment of *Arthrospira* compounds as potential antiviral agents against SARS-CoV-2. *J. Appl. Phycol.* **2021**, *33*, 1579–1602. [CrossRef]
39. Pierson, T.C.; Diamond, M.S. The continued threat of emerging flaviviruses. *Nat. Microbiol.* **2020**, *5*, 796–812. [CrossRef]
40. Li, J.; Lai, S.; Gao, G.F.; Shi, W. The emergence, genomic diversity and global spread of SARS-CoV-2. *Nature* **2021**, *600*, 408–418. [CrossRef]
41. Stawicki, S.P.; Jeanmonod, R.; Miller, A.C.; Paladino, L.; Gaieski, D.F.; Yaffee, A.Q.; De Wulf, A.; Grover, J.; Papadimos, T.J.; Bloem, C.; et al. The 2019-2020 novel coronavirus (severe acute respiratory syndrome coronavirus 2) pandemic: A joint American College of Academic International Medicine-World Academic Council of Emergency Medicine Multidisciplinary COVID-19 Working Group Consensus Paper. *J. Glob. Infect. Dis.* **2020**, *12*, 47–93. [CrossRef]
42. Hoffmann, M.; Kleine-Weber, H.; Schroeder, S.; Krüger, N.; Herrler, T.; Erichsen, S.; Schiergens, T.S.; Herrler, G.; Wu, N.-H.; Nitsche, A.; et al. SARS-CoV-2 cell entry depends on ACE2 and TMPRSS2 and is blocked by a clinically proven protease inhibitor. *Cell* **2020**, *181*, 271–280.e8. [CrossRef] [PubMed]
43. Synowiec, A.; Jedrysik, M.; Branicki, W.; Klajmon, A.; Lei, J.; Owczarek, K.; Suo, C.; Szczepanski, A.; Wang, J.; Zhang, P.; et al. Identification of cellular factors required for SARS-CoV-2 replication. *Cells* **2021**, *10*, 3159. [CrossRef] [PubMed]
44. Klemm, T.; Ebert, G.; Calleja, D.J.; Allison, C.C.; Richardson, L.W.; Bernardini, J.P.; Gc Lu, B.; Kuchel, N.W.; Grohmann, C.; Shibata, Y.; et al. Mechanism and inhibition of the papain-like protease, $PL^{pro}$, of SARS-CoV-2. *EMBO J.* **2020**, *39*, e106275. [CrossRef] [PubMed]
45. Clemente, V.; D'Arcy, P.; Bazzaro, M. Deubiquitinating enzymes in coronaviruses and possible therapeutic opportunities for COVID-19. *Int. J. Mol. Sci.* **2020**, *21*, 3492. [CrossRef]
46. Huynh, T.; Cornell, W.; Luan, B. In silico exploration of inhibitors for SARS-CoV-2's papain-like protease. *Front. Chem.* **2021**, *8*, 624163. [CrossRef]
47. Zhao, Y.; Du, X.; Duan, Y.; Pan, X.; Sun, Y.; You, T.; Han, L.; Jin, Z.; Shang, W.; Yu, J.; et al. High-throughput screening identifies established drugs as SARS-CoV-2 $PL^{pro}$ inhibitors. *Protein Cell* **2021**, *12*, 877–888. [CrossRef]
48. Liang, X.; Kaya, A.; Zhang, Y.; Tien Le, D.; Hua, D.; Gladyshev, V.N. Characterization of methionine oxidation and methionine sulfoxide reduction using methionine-rich cysteine-free proteins. *BMC Biochem.* **2012**, *13*, 21. [CrossRef]
49. Kim, G.; Weiss, S.J.; Levine, R.L. Methionine oxidation and reduction in proteins. *Biochim. Biophys. Acta* **2014**, *1840*, 901–905. [CrossRef]
50. Shoombuatong, W.; Schaduangrat, N.; Nantasenamat, C. Unraveling the bioactivity of anticancer peptides as deduced from machine learning. *EXCLI J.* **2018**, *17*, 734–752. [CrossRef]
51. Sakib, M.M.H.; Nishat, A.A.; Islam, M.T.; Raihan Uddin, M.A.; Iqbal, M.S.; Bin Hossen, F.F.; Ahmed, M.I.; Bashir, M.S.; Hossain, T.; Tohura, U.S.; et al. Computational screening of 645 antiviral peptides against the receptor-binding domain of the spike protein in SARS-CoV-2. *Comput. Biol. Med.* **2021**, *136*, 104759. [CrossRef]
52. Chowdhury, S.M.; Talukder, S.A.; Khan, A.M.; Afrin, N.; Ali, M.A.; Islam, R.; Parves, R.; Al Mamun, A.; Sufian, M.A.; Hossain, M.N.; et al. Antiviral peptides as promising therapeutics against SARS-CoV-2. *J. Phys. Chem. B* **2020**, *124*, 9785–9792. [CrossRef] [PubMed]
53. Huang, K.Y.; Tseng, Y.J.; Kao, H.J.; Chen, C.H.; Yang, H.H.; Weng, S.L. Identification of subtypes of anticancer peptides based on sequential features and physicochemical properties. *Sci. Rep.* **2021**, *11*, 13594. [CrossRef] [PubMed]
54. Dai, Y.; Cai, X.; Shi, W.; Bi, X.; Su, X.; Pan, M.; Li, H.; Lin, H.; Huang, W.; Qian, H. Pro-apoptotic cationic host defense peptides rich in lysine or arginine to reverse drug resistance by disrupting tumor cell membrane. *Amino Acids* **2017**, *49*, 1601–1610. [CrossRef]
55. Chiangjong, W.; Chutipongtanate, S.; Hongeng, S. Anticancer peptide: Physicochemical property, functional aspect and trend in clinical application (Review). *Int. J. Oncol.* **2020**, *57*, 678–696. [CrossRef] [PubMed]
56. Pettit, G.R.; Kamano, Y.; Herald, C.L.; Tuinman, A.A.; Boettner, F.E.; Kizu, H.; Schmidt, J.M.; Baczynskyj, L.; Tomer, K.B.; Bontems, R.J. The isolation and structure of a remarkable marine animal antineoplastic constituent: Dolastatin 10. *J. Am. Chem. Soc.* **1987**, *109*, 6883–6885. [CrossRef]
57. Thornburg, C.C.; Cowley, E.S.; Sikorska, J.; Shaala, L.A.; Ishmael, J.E.; Youssef, D.T.; McPhail, K.L. Apratoxin H and apratoxin A sulfoxide from the Red Sea cyanobacterium *Moorea producens*. *J. Nat. Prod.* **2013**, *76*, 1781–1788. [CrossRef] [PubMed]
58. Trimurtulu, T.; Ohtani, I.; Patterson, G.M.L.; Moore, R.E.; Corbett, T.H.; Valeriote, F.A.; Demchik, L. Total structures of cryptophycins, potent antitumor depsipeptides from the blue-green alga *Nostoc* sp. Strain GSV 224. *J. Am. Chem. Soc.* **1994**, *116*, 4729–4737. [CrossRef]

59. Kaneda, M.; Kawaguchi, S.; Fujii, N.; Ohno, H.; Oishi, S. Structure-activity relationship study on odoamide: Insights into the bioactivities of aurilide-family hybrid peptide-polyketides. *ACS Med. Chem. Lett.* **2018**, *9*, 365–369. [CrossRef]
60. Simmons, T.L.; McPhail, K.L.; Ortega-Barría, E.; Mooberry, S.L.; Gerwick, W.H. Belamide A, a new antimitotic tetrapeptide from a Panamanian marine cyanobacterium. *Tetrahedron Lett.* **2006**, *47*, 3387–3390. [CrossRef]
61. Cegłowska, M.; Toruńska-Sitarz, A.; Stoń-Egiert, J.; Mazur-Marzec, H.; Kosakowska, A. Characteristics of cyanobacterium *Pseudanabaena galeata* CCNP1313 from the Baltic Sea. *Algal Res.* **2020**, *47*, 101861. [CrossRef]
62. Jin, Z.; Du, X.; Xu, Y.; Deng, Y.; Liu, M.; Zhao, Y.; Zhang, B.; Li, X.; Zhang, L.; Peng, C.; et al. Structure of $M^{pro}$ from SARS-CoV-2 and discovery of its inhibitors. *Nature* **2020**, *582*, 289–293. [CrossRef] [PubMed]
63. Osipiuk, J.; Azizi, S.-A.; Dvorkin, S.; Endres, M.; Jedrzejczak, R.; Jones, K.A.; Kang, S.; Kathayat, R.S.; Kim, Y.; Lisnyak, V.G.; et al. Structure of papain-like protease from SARS-CoV-2 and its complexes with non-covalent inhibitors. *Nat. Commun.* **2021**, *12*, 743. [CrossRef] [PubMed]
64. Owen, D.R.; Allerton, C.M.N.; Anderson, A.S.; Aschenbrenner, L.; Avery, M.; Berritt, S.; Boras, B.; Cardin, R.D.; Carlo, A.; Coffman, K.J.; et al. An oral SARS-CoV-2 $M^{pro}$ inhibitor clinical candidate for the treatment of COVID-19. *Science* **2021**, *374*, 1586–1593. [CrossRef] [PubMed]